Cilostazol Inhibits Oxidative Stress–Induced Premature Senescence Via Upregulation of Sirt1 in Human Endothelial Cells

Hidetaka Ota, Masato Eto, Mitsunobu R. Kano, Sumito Ogawa, Katsuya Iijima, Masahiro Akishita, Yasuyoshi Ouchi

Objective—Cilostazol, a selective inhibitor of PDE3, has a protective effect on endothelium after ischemic vascular damage, through production of nitric oxide (NO). The purpose of the present study was to clarify the molecular mechanisms underlying the preventive effect of treatment with cilostazol on oxidative stress–induced premature senescence in human endothelial cells.

Methods and Results—Prematurely senescent human umbilical vein endothelial cells (HUVECs) were induced by treatment with hydrogen peroxide (H_2O_2) as judged by senescence-associated β-galactosidase assay (SA-βgal), cell morphological appearance, and plasminogen activator inhibitor-1 (PAI-1) expression. Treatment with H_2O_2 caused 93% of the cells to be SA-βgal positive, whereas 46% of cilostazol (100 μmol/L)-treated cells were positive. HUVECs treated with other cAMP-elevating agents and DETA-NO showed a reduction of SA-βgal–positive cells as well. Cilostazol increased phosphorylation of Akt at Ser^{473} and of endothelial nitric oxide synthase (eNOS) at Ser^{1177}, with a dose-dependent increase in Sirt1 expression. Moreover, the effect of cilostazol on premature senescence was abrogated through inhibition of Sirt1.

Conclusions—Our results indicated that cilostazol exerted protective effects against endothelial senescence and dysfunction, and enhancement of NO production is a key mediator in upregulation of Sirt1. (***Arterioscler Thromb Vasc Biol.* 2008;28:1634-1639**)

Key Words: cilostazol ■ eNOS ■ Sirt1 ■ endothelial senescence

The phenomenon of human aging is known to be a critical cardiovascular risk factor. Cellular senescence of endothelial cells has been proposed to be involved in endothelial dysfunction and atherogenesis.[1] The lesions of human atherosclerosis have been extensively studied histologically, and these studies have demonstrated that there are vascular cells that exhibit the morphological features of cellular senescence.[2]

See accompanying article on page 1577

The telomere hypothesis is a widely accepted explanation of the occurrence of cellular senescence.[3] Cessation of cell division after extended propagation in culture for a few weeks or months is related to the attrition of telomeres, which is termed replicative senescence. In addition to telomere attrition, some stressors such as oxidative stress elicit similar growth arrest within just a few days, referred to as stress-induced premature senescence (SIPS). Both types of senescence are accompanied by a specific set of changes in cell function, morphology, and gene expression.[4] In addition to the above changes, recognized biomarkers of senescent cells include staining for β-galactosidase at pH of 6.0 as opposed to endogenous lysosomal enzyme detected at pH of 4.0 in normal cells.[5]

According to the free-radical theory, reactive oxygen species (ROS) may be potential candidates responsible for senescence and age-related diseases, and on production of high levels of ROS, the redox balance is disturbed and cells shift into a state of oxidative stress, which subsequently leads to premature senescence with shortening telomeres.[6]

A PDE3 inhibitor, cilostazol, is used as a vasodilating antiplatelet drug for treating intermittent claudication, and in preclinical studies was shown to have a protective effect on endothelial cells by increasing eNOS activity.[7] Cilostazol increases intracellular cAMP content accordingly and activates protein kinase A (PKA) or PI3K/Akt signaling.[8] As recently shown, endothelial NO can protect against a state of oxidative stress, and activation of eNOS and subsequent production of NO delay endothelial cellular senescence.[9,10]

In yeast, Sir2 (silent information regulator-2) has been identified as an NAD^+-dependent histone deacetylase.[11]

Original received February 4, 2008; final version accepted May 28, 2008.

From the Departments of Geriatric Medicine (H.O., M.E., S.O., K.I., M.A., Y.O.) and Molecular Pathology (M.R.K.), Graduate School of Medicine, University of Tokyo, Japan.

Correspondence to Yasuyoshi Ouchi, MD, PhD, Department of Geriatric Medicine, Graduate School of Medicine, The University of Tokyo, 7-3-1 Hongo, Bunkyo-ku, Tokyo 113-8655, Japan. E-mail youchi-tky@umin.ac.jp

Arterioscler Thromb Vasc Biol is available at http://atvb.ahajournals.org

DOI: 10.1161/ATVBAHA.108.164368

Mammalian sirtuin 1 (Sirt1), the closest homolog of Sir2, regulates the cell cycle, senescence, apoptosis, and metabolism, by interacting with a number of molecules, including p53, PML, and PPAR-γ.[12–14] A recent study showed that production of NO by caloric restriction increases Sirt1 expression and suggested that eNOS may be involved in regulating the expression of Sirt1 in murine white adipocytes.[15] Therefore, we consider that the protective effect of cilostazol against vascular senescence may be attributed to upregulation of Sirt1.

In the present study, cilostazol inhibited oxidative stress–induced premature senescence, and the increased expression of Sirt1 by this drug played a critical role in prevention of endothelial senescence.

Materials and Methods

Cilostazol was kindly provided by Otsuka Pharmaceutical Co Ltd, Tokyo, Japan. Forskolin, rolipram, N^G-nitro-L-arginine methyl ester hydrochloride (L-NAME) and LY294002 were purchased from Sigma. Myristoylated cell-permeable PKA inhibitor peptide sequence[14–22] amide (PKAI) was from Alexis Biochemicals. (Z)-1-[2-(2-aminoethyl)-N-(2-ammonioethyl)amino] diazen-1-IM1,2 diolate (DETA-NO), S-nitrosoacetyl penicillamine (SNAP), 8 Br-cGMP, and 8 Br-cAMP were from Cayman Chemical. *N*-acetyl-cystein (NAC) was purchased from Calbiochemo.

Cell Culture

Human umbilical vein endothelial cells (HUVECs) were purchased from CAMBREX (Walkersville, Md), and maintained in endothelial growth medium (EGM-2, EGM-2 singleQuots, CAMBREX). Population doubling levels (PDL) were calculated as described previously,[16] and all experiments were performed at PDL of 8 to 9.

Measurement of cAMP Level

HUVECs were plated in 96-well plates at a density of 5×10^3 cells per well and cultured overnight. After 15-minute incubation with cilostazol, the medium was aspirated and a lysis buffer was added. cAMP concentration was determined using a cAMP EIA kit (Amersham Biosciences) according to the manufacturer's instructions.

Inhibition of Sirt1

Proliferating cells were washed 3 times with growth medium and exposed for 24 hours to the indicated concentrations of sirtinol (Calbiochem) or nicotinamide (NAM, Wako Chemical Industries) diluted in medium. After exposure, the dishes were washed 3 times with inhibitor-free medium and cultured. Proliferating cells were transfected with 200 pmol/L siRNA for Sirt1 (GAT GAA GTT GAC CTC CTC A[14] and TGA AGT GCC trichloroacetic acid (TCA) GAT ATT A) or control siRNA (Darmacom Co.) using silMPORTER (Upstate Cell Signaling Solutions).

Senescence-Associated β-Galactosidase (SA-βgal) Staining

HUVECs were grown in 100-mm collagen-coated dishes to 80% confluence. HUVECs were pretreated with vehicle (0.05% DMSO), cilostazol (1 to 100 μmol/L), forskolin (0.1 to 1 μmol/L), rolipram (10 to 100 μmol/L), DETA-NO (50, 100 μmol/L), or NAC (3, 5 mmol/L) diluted in EGM-2 medium for 3 days. HUVECs were washed 3 times with EGM-2 and then treated for 1 hour with 100 μmol/L H_2O_2 diluted in EGM-2. After the treatment, HUVECs were trypsinized, reseeding at the density of 1×10^5 in 60-mm dishes and cultured with EGM-2 containing these compounds for 10 days. At 10 days after treatment with H_2O_2, HUVECs were fixed and the proportion of SA-βgal–positive cells was determined as described by Dimri et al.[5]

NOS Activation Assay

NOS activity was determined using an NOS assay kit (Calbiochem) according to the manufacturer's instructions.

BrdU Incorporation Assay

BrdU incorporation was analyzed using a commercial kit (Roche).

Immunoblotting

Cells were lysed on ice for 1 hour in buffer (50 mmol/L Tris-HCl, pH 7.6, 150 mmol/L NaCl, 1%NP-40, 0.1%SDS, 1 mmol/L dithiothreitol, 1 mmol/L sodium vanadate, 1 mmol/L phenylmethylsulfonyl fluoride, 10 μg/mL aprotinin, 10 μg/mL leupeptin, and 10 mmol/L sodium fluoride). Equal amounts of protein were separated by SDS-polyacrylamide gel electrophoresis and transferred to nitrocellulose membranes. After blocking, the filters were incubated with the following antibodies; antiphospho-eNOS (Ser1177), antiphospho-Akt (Ser473), anti-Akt (Cell Signaling Technology), antieNOS (BD Transduction Laboratories), antiacetyl-p53 (Lys373/382), antip53, anti-Sirt1 (Santa Cruz Biotechnology Inc), anti-PAI-1 (Molecular Innovations Inc), and anti-β-actin (Sigma). After washing and incubation with horseradish peroxidase-conjugated antirabbit or antimouse IgG (Amersham) for 1 hour, the antigen-antibody complexes were visualized using an enhanced chemiluminescence system (Amersham).

Real-Time Quantitative Reverse Transcription

Expression of Sirt1 in HUVECs was measured by quantitative RT-polymerase chain reaction (PCR). Total RNA in HUVECs was isolated with ISOGEN (Nippon gene Inc). After treatment with Rnase-free Dnase for 30 minutes, total RNA (50 ng/μL) was reverse transcribed with random hexamers and oligo d(T) primers. The expression level of Sirt1 relative to GAPDH was determined by means of staining with SYBR green dye and a LineGene fluorescent quantitative detection system (Bioflux Co), as recommended by the manufacturer. Primer quality was verified by dissociation curve analysis, the slopes of standard curves, and reactions without RT. The following primers were used: Sirt1 (forward (F) 5′-CCTGACTTCAGATCAAGAGACGGT-3′; reverse (R) 5′-CTGATTAAAAATGTCTCCACGAACAG-3′, GAPDH F 5′-ACCACAGTCCATGCCATCAC-3′; R 5′-TCCACCACCCTGTTGCTGTA-3′).

Animal Experiments

The animal experiments were approved by our institutional review board. Ten-week-old SPF male wild-type BALB/c mice (n=40, weighing approximately 25 g) were supplied by Charles River Laboratories Inc. Animals were housed under a 12-hour light/dark cycle and fed a normal diet. These mice were administered 25 mg/kg paraquat (1,1-dimethyl-4,4-bipyridinium) (Wako Chemical) by intraperitoneal injection. Then mice were randomly assigned to 2 treatment groups (control group, n=20; cilostazol group, n=20). The each group received gavage administration of vehicle alone or cilostazol 60 mg/kg/d for their lifetime. We made diabetic mice (n=40) by a single intraperitoneal injection of streptozotocin (STZ; 60 mg/kg, Sigma). Tail blood glucose was assayed 3 days after injection using glucose test strips (Roche). The mice were killed by cervical dislocation. The aorta was removed after systemic perfusion with phosphate-buffered saline (PBS) for histological examination. The proportion of SA-βgal–positive cells was analyzed by NIH image software. The primary antibody was purified rat antimouse CD31 (platelet endothelial cell adhesion molecule; PECAM-1) monoclonal antibody from pharmingen. ROS were measured with 2′, 7′-Dichlorodihydrofluorescein, diacetate (DCF) (Sigma). As previously described by Shi et al,[17] the aorta was rapidly removed and placed in oxygenated (12% O_2, 5% CO_2) physiological salt solution (PSS) of the following composition (NaCl 130 mmol/L, KCl 4.7 mmol/L, $CaCl_2$ 1.6 mmol/L, $MgSO_4$ 1.17 mmol/L, $NaHCO_3$ 14.9 mmol/L, KH_2PO_4 1.18 mmol/L, EDTA 0.026 mmol/L, glucose 1.0 mmol/L). The living aorta was carefully isolated, cannulated (24G, Terumo Co Ltd) at both ends, pressured, and loaded with DCF solution (10 μmol/L) for 10 minutes. Then the aorta was washed by PSS 3 times, embedded in OCT medium, and cryosectioned.

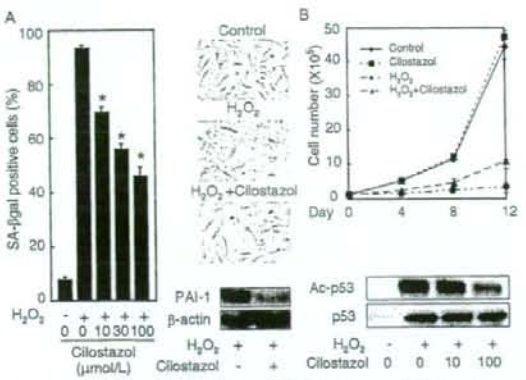

Figure 1. A, Cilostazol inhibited H_2O_2 (100 μmol/L)-induced premature senescent phenotype in HUVECs as judged by SA-βgal staining (*$P<0.05$, n=3), morphological changes, and PAI-1. B, Cell growth curve, acetylation of p53 (Ac-p53) at lysine 373/382, and total protein of p53 were evaluated at 10 days after addition of H_2O_2.

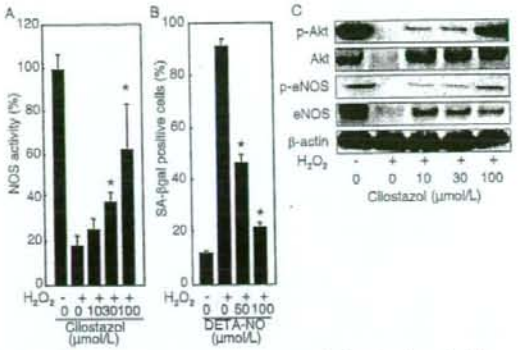

Figure 2. A, NOS activity was measured after treatment with cilostazol. B, DETA-NO inhibited H_2O_2 (100 μmol/L)-induced premature senescent phenotype in HUVECs as judged by SA-βgal staining. (*$P<0.05$, n=3). C, Expression of phospho-eNOS (Ser1177), phospho-Akt (Ser473), Akt, and eNOS in cilostazol-treated cells.

TOTO-3 for nuclear staining, secondary antibodies (Alexa Fluor 488 donkey antirat IgG and Alexa Fluor 594 donkey antirat IgG), and antifade reagent were from Molecular Probe (Invitrogen). Fluorescent images were taken and analyzed using a confocal laser microscope (LSM510, Carl Zeiss MicroImaging Co Ltd). Urinary 8-Hydroxydeoxyguanosine (8-OhdG) and creatinine were measured using a DNA damage ELISA kit (Stressgen) and creatinine assay kit (Cayman chemical), respectively.

Telomerase Assay

Telomerase activity was measured with 2 μg protein using a telomerase PCR-ELISA kit according to the manufactures instructions (Chemicon, Temecula).

Data Analysis

Values are shown as mean±SEM in the text and figures. Differences between the groups were analyzed using 1-way analysis of variance, followed by Bonferroni test. Probability values less than 0.05 were considered significant.

Results

Cilostazol Inhibits Oxidative Stress–Induced Premature Senescence in Human Endothelial Cells

To investigate the effect of cilostazol on the senescent phenotype in HUVECs, we induced premature endothelial senescence by addition of H_2O_2 100 μmol/L for 1 hour. We found that treatment with cilostazol inhibited the senescent phenotype as judged by SA-βgal assay and enlarged and flattened cell morphological appearance at 10 days. Under treatment with H_2O_2, 93% of cells were SA-βgal positive, versus only 46% of cilostazol (100 μmol/L)-treated cells under the same oxidative conditions (Figure 1A). We found that HUVECs treated with other cAMP-elevating agents showed a reduction of SA-βgal–positive cells as well (forskolin 1 μmol/L; 51%, rolipram 100 μmol/L; 53%). Treatment with cilostazol decreased the specific senescent morphological changes (Figure 1A). Expression of PAI-1 was decreased by treatment with cilostazol (Figure 1A). Treatment with cilostazol restored the rate of BrdU incorporation in prematurely senescent HUVECs (supplemental Figure I, available online at http://atvb.ahajournals.org). In parallel with this, telomerase activity was increased by treatment with cilostazol (supplemental Figure I). Moreover, we examined the effect on cell growth for 12 days after treatment with vehicle, H_2O_2 and cilostazol. Addition of H_2O_2 decreased cell number of HUVECs and treatment with cilostazol recovered it (Figure 1B). p53 plays a pivotal role in cellular senescence. Therefore, we examined the expression and acetylation of p53 at Lys373/382, one of the critical targets of Sirt1. As shown in Figure 1B, we observed that H_2O_2 increased the expression and acetylation of p53, and treatment with cilostazol decreased the acetylation of p53.

Enhancement of cAMP Production and eNOS Activity Induced by Cilostazol

When HUVECs were treated with cilostazol, the cAMP level significantly increased in a concentration-dependent manner at cilostazol concentrations of 1 and 100 μmol/L (data not shown). In the presence of H_2O_2, cilostazol increased eNOS activity (Figure 2A), expression of eNOS, and the phosphorylation of eNOS at Ser^{1177} in parallel with the phosphrylation of Akt at Ser^{473} (Figure 2C). Although exposure to H_2O_2 affected the total amount of eNOS and Akt, treatment with cilostazol reverted their expression to nearly normal levels (Figure 2C). To investigate the effect of NO on the senescent phenotype in HUVECs, we treated these cells with an NO donor, DETA-NO (100 μmol/L). DETA-NO–treated HUVECs showed decreased SA-βgal–positive cells (Figure 2B), and an increased rate of BrdU incorporation and telomerase activity (supplemental Figure I). These results suggest that the protective effect against a senescent phenotype may be attributed to an increased of NO via eNOS activation by cilostazol.

Treatment With Cilostazol Increased Sirt1 Expression

To explore the mechanism by which cilostazol prevents from premature endothelial senescence, we considered that an increase in NO production could promote the longevity gene,

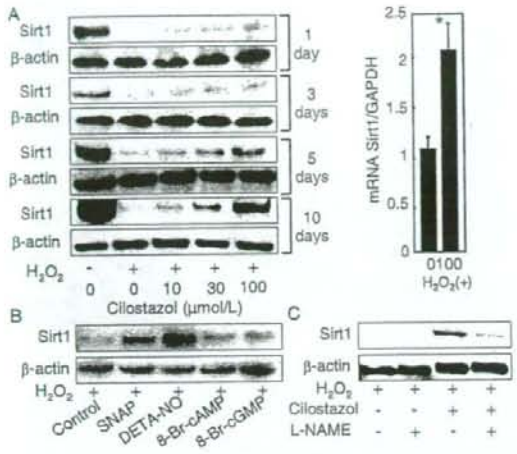

Figure 3. A, Sirt1 protein and mRNA in the presence of H_2O_2 (100 μmol/L). Sirt1 expression was increased by treatment with SNAP (100 μmol/L), DETA-NO (50 μmol/L), 8 Br-cGMP (1 mmol/L), or 8 Br-cAMP (1 mmol/L) (B) and decreased by treatment with L-NAME (20 μmol/L) for 6 hours (C). *$P<0.05$.

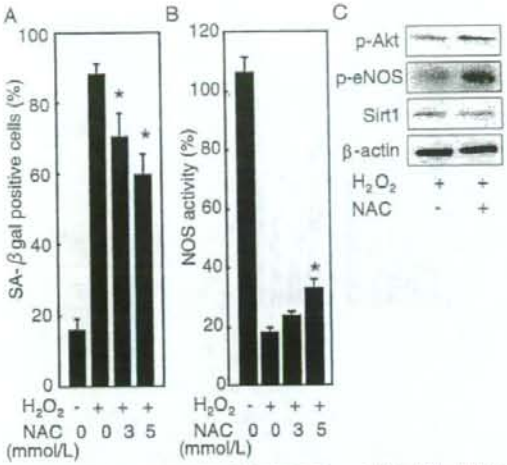

Figure 4. A, Treatment with NAC (0, 3, 5 mmol/L) inhibited H_2O_2 (100 μmol/L)-induced premature senescent phenotype in HUVECs as judged by SA-βgal staining (n=3). B, NOS activity after treatment with NAC. C, Expression of phospho-eNOS (Ser1177), phospho-Akt (Ser473), and Sirt1 in NAC (5 mmol/L)-treated cells. *$P<0.05$.

Sirt1. We found that cilostazol significantly increased Sirt1 mRNA and protein in a concentration-dependent manner for 10 days after treatment with H_2O_2 (Figure 3A). In contrast, Sirt1 mRNA and protein were not altered in the absence of H_2O_2 treatment (data not shown). To determine whether the expression of Sirt1 was regulated by the increase in NO production, we exposed prematurely senescent HUVECs to either an NO donor (such as DETA-NO or SNAP), a cAMP analog (8 Br-cAMP), or a cGMP analog (8 Br-cGMP). After these treatments, the expression of Sirt1 protein was markedly higher than that in untreated cells (Figure 3B). Furthermore, treatment with an NOS inhibitor, L-NAME, decreased Sirt1 expression (Figure 3C). To clarify the molecular mechanisms by which cilostazol induces SIRT1 expression, we examined the effect of protein kinase inhibitors on the cilostazol-induced phosphrylation of eNOS, Akt and expression of Sirt1 (supplemental Figure II). In the absence of H_2O_2 treatment, PKAI and LY294002 inhibited the cilostazol-induced phosphorylation of eNOS at Ser^{1177}. The cilostazol-induced phosphorylation of Akt at Ser^{473} was inhibited by LY294002, however the inhibition by PKAI was not significant. Sirt1 expression was not altered by treatment with PKAI or LY294002. In the presence of H_2O_2 treatment, PKAI and LY294002 showed the similar effect on the cilostazol-induced phosphorylation of eNOS at Ser^{1177} and Akt at Ser^{473}, but Sirt1 expression was significantly decreased.

Cilostazol Dose Not Have a Function of Direct Scavenger of Hydrogen Peroxide

It is possible that cilostazol may function as an antioxidant drug. Therefore, we examined the effect of NAC, another antioxidant, on Sirt1 expression, phosphorylation of Akt, and NOS activity as well as senescence markers. As shown in Figure 4A, treatment with NAC (0, 3, 5mmol/L) significantly decreased SA-βgal activity. Phosphorylation of Akt and NOS activity was increased by treatment with NAC (Figure 4B and 4C). However, Sirt1 expression was not altered (Figure 4C). To clarify the effect of cilostazol or NAC on H_2O_2, we examined whether cilostazol or NAC could scavenge H_2O_2 radicals. We performed a cell-free, horseradish peroxidase–coupled oxidation analysis.[18] We observed that NAC scavenged H_2O_2 significantly, but cilostazol not (supplemental Figure III). These results indicate that inhibiting H_2O_2-induced senescence by cilostazol may not be attributable to its direct antioxidative effect such as NAC.

Inhibition of Sirt1 Abrogates the Protective Effect of Cilostazol Against Premature Senescence

To determine the role of endogenous Sirt1 in premature senescence, HUVECs were treated with a Sirt1 chemical inhibitor, sirtinol, a physiological Sirt1 inhibitor, NAM or Sirt1 siRNA. Knockdown of Sirt1 with siRNA was confirmed by Western blotting. As shown in Figure 5A and 5B, Sirt1 inhibition abrogates the effect of cilostazol on SA-βgal activity and the senescent specific morphological changes. Likewise, we found that Sirt1 inhibition had a similar effect to DETA-NO treatment (data not shown). Increased phosphorylation of eNOS at Ser^{1177} and decreased expression of PAI-1 by cilostazol were no longer observed when Sirt1 was inhibited (Figure 5C). These results indicate that Sirt1 could play an important role in the protective effect of cilostazol against a senescent phenotype.

Administration of Cilostazol Inhibits Vascular Endothelial Senescence Induced by Oxidative Stress in BALB/c Mice

To investigate whether cilostazol has a protective effect on vascular endothelial senescence induced by oxidative stress in vivo, we administrated paraquat, a herbicide that generates

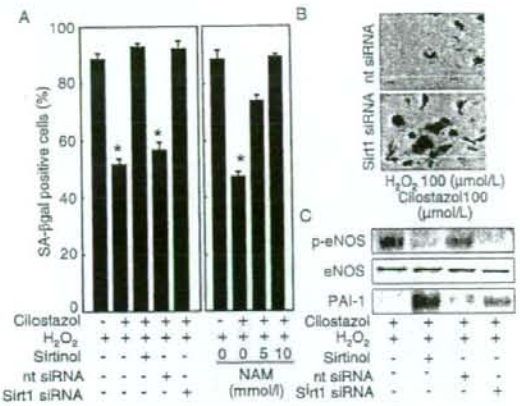

Figure 5. Inhibition of Sirt1 abrogates effect of cilostazol (100 μmol/L) against a premature senescence phenotype as shown by SA-βgal staining (n=3) (A), morphological changes (B), and expression of phospho-eNOS (Ser1177) and PAI-1 (C). Sirt1 was inhibited by sirtinol (100 μmol/L), NAM (5, 10 mmol/L), or Sirt1 siRNA. nt indicates nontargeted. *$P<0.05$.

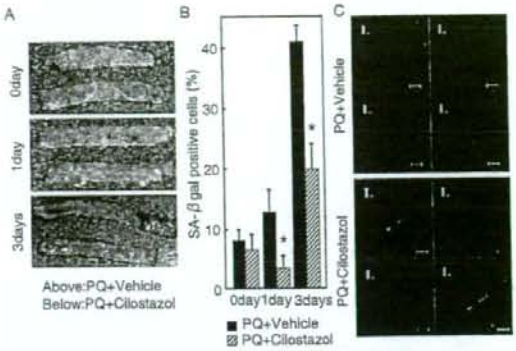

Figure 6. A, SA-βgal staining of thoracic arteries from BALB/c mice with cilostazol at 0, 1, and 3 days after treatment with paraquat (PQ). B, The number of SA-βgal staining cells in cilostazol-treated thoracic arteries. C, Immunofluorescent staining for Sirt1 (green), PECAM-1 (red), and TOTO-3 (blue). Representative samples (n=40) shown. *$P<0.05$.

superoxide, to BALB/c mice. We performed resection of the thoracic artery of these mice and compared the senescent phenotype in the presence and absence of cilostazol. The number of SA-βgal–staining cells was significantly increased in untreated thoracic arteries, but was decreased in cilostazol-treated thoracic arteries (Figure 6A and 6B). Cross-sections of arteries stained with SA-βgal showed that positive cells were mostly located on the luminal surface and stained for CD-31, indicating that blue staining originated from vascular endothelial cells and not from the extracellular matrix (supplemental Figure IV). To estimate the degree of DNA damage caused by paraquat, we measured urinary 8-OhdG, a marker of DNA damage from oxidative stress. Urinary 8-OHdG level was decreased after cilostazol treatment (supplemental Figure IV). Immunostaining of the sections for Sirt1 showed that Sirt1 expression was increased in aortic endothelial cells by treatment with cilostazol (Figure 6C). To estimate the antioxidative effect of cilostazol on vasculature, we used DCF, cell-permeable fluorogenic probe, to measure ROS within cells by detection of enzymatically formed H_2O_2. The intensity of green fluorescence indicating DCF-positive cells was markedly increased in untreated thoracic arteries, which was decreased in cilostazol-treated thoracic arteries (supplemental Figure IV). The number of DCF-positive endothelial cells was decreased in cilostazol-treated thoracic arteries (supplemental Figure IV). Next, we used STZ diabetic mice in which the endothelial senescence documented.[19] The treatment with cilostazol decreased SA-βgal–positive endothelial cells (supplemental Figure V).

Discussion

As previously reported,[20] the concentration of cilostazol (60 mg/kg/d) we administrated in this study was within clinical relevance. In vitro experiments, we used cilostazol at 0 to 100 μmol/L and confirmed a concentration-dependent trend. Given the average plasma concentration of cilostazol orally administered to humans (100 mg/body/d) is about 2 to 10 μmol/L and may be partially higher in our body, our used concentration of cilostazol is comparable to clinical.

Previous studies have shown that overexpression of Sirt1 antagonizes cellular senescence through acetylation of p53 with localization of the PML body.[13] Recently, we reported that Sirt1 overexpression prevented the development of oxidative stress–induced premature senescence in human endothelial cells.[21] Senescence of endothelial cells leads to endothelial dysfunction and may result in advanced atherosclerotic lesions.[2] In fact, it has been reported that endothelial cells in samples of human aortia with atherosclerosis exhibited a senescence-like phenotype, increased expression of PAI-1,[22] and decreased production of NO.[1] NO production and eNOS expression are severely limited in senescent endothelial cells.[23] Although NO is known to be involved in reducing oxidative stress and the progression of atheroscrerosis, the present study suggested that the NO-mediated prevention of premature senescence was attributable to Sirt1 function. These findings implicate the NO-Sirt1 axis as one of the fundamental determinants of endothelial senescence, and the role of Sirt1 as a driver of cellular stress resistance and longevity is noteworthy in the context of its expression profile.

The free-radical theory of aging proposes that degenerative senescence is largely the result of the cumulative effect of ROS. In this study, we used paraquat mice as an oxidative stress model. Moreover, we studied the effect of cilostazol on endothelial senescence used by STZ-diabetic mice as more suitable for clinical settings. In addition, Takase et al recently reported that cilostazol had exhibited an antiatherosclerotic effect on vasculature in ApoE-deficient mice.[24] Therefore, we suggest that cilostazol has a beneficial effect on vasculature in clinical settings.

Cilostazol-induced NO production by eNOS activation via a cAMP/PKA- and PI3K/Akt-dependent mechanism was previously confirmed in the porcine thoracic aorta by an ESR[25] technique and in clinical practice by endothelial-dependent vasodilation.[26] Our results showed that cilostazol phosphorylated Akt via a PKA-independent mechanism (sup-

plemental Figure II). It is suggested that both cAMP/PKA and PI3K/Akt signaling pathways are involved in cilostazol-induced phosphorylation of eNOS, however the contribution of these signaling to the upregulation of Sirt1 in the presence of H_2O_2 is more critical than that of in the absence of H_2O_2. Therefore, we suggest that upregulation of Sirt1 by cilostazol is modulated via cAMP/PKA, PI3K/Akt, and eNOS-dependent mechanism under oxidative conditions, but further investigation is needed to elucidate why there is discrepancy of Sirt1 expression.

A recent study showed DETA-NO, an NO-donor, and eNOS transfection activated hTERT and delayed endothelial senescence, indicating that eNOS has an antiatherosclerotic effect even in cases of advanced atherosclerosis. It is therefore suggested that incrased NO bioavailability by other pharmaceutical products such as 3-hydroxy-3-methylglutaryl (HMG)-coenzyme A (CoA) reductase inhibitors or agents with phytoestrogenic properties such as resveratrol may exert a protective effect against endothelial senescence, and this possibility deserves further investigation.

In summary, we showed that cilostazol inhibited oxidative stress–induced premature senescence, and subsequently enhancement of Sirt1 expression played a critical role in inhibition of a senescent phenotype in human endothelial cells. Our results suggest that NO production by cilostazol has a protective effect against endothelial senescence and dysfunction.

Sources of Funding

This work was supported by a Grant-in-Aid for Scientific Research from the Ministry of Education, Science, Culture and Sports of Japan (18590801).

Disclosures

None.

References

1. Minamino T, Miyauci H, Yoshida T, Ishida Y, Yoshida H, Komuro I. Endothelial cell senescence in human atherosclerosis: role of telomere in endothelial dysfunction. *Circulation*. 2002;105:1541–1544.
2. Burrig KF. The endothelium of advanced arteriosclerotic plaques in humans. *Arterioscler Thromb*. 1991;11:1678–1689.
3. Liu JP. Studies of the molecular mechanisms in the regulation of telomerase activity. *FASEB J*. 1999;13:2091–2104.
4. Yang J, Chang E, Cherry AM, Bangs CD, Oei Y, Bodnar A, Bronstein A, Chiu CP, Herron GS. Human endothelial cell life extension by telomerase expression. *J Biol Chem*. 1999;274:26141–26148.
5. Dimri GP, Lee X, Basile G, Acosta M, Scott G, Roskelley C, Medrano EE, Linskens M, Rubelj I, Pereira-Smith O, et al. A biomarker that identifies senescent human cells in culture and in aging skin in vivo. *Proc Natl Acad Sci USA*. 1995;92:9363–9367.
6. Kurz DJ, Decary S, Hong Y, Trivier E, Akhmedov A, Erusalimsky JD. Chronic oxidative stress compromises telomere integrity and accelerates the onset of senescence in human endothelial cells. *J Cell Sci*. 2004;117:2417–2426.
7. Kambayashi J, Liu Y, Sun B, Shakur Y, Yoshitake M, Czerwiec F. Cilostazol as a unique antithrombotic agent. *Curr Pharm Des*. 2003;9:2289–2302.
8. Hashimoto A, Miyakoda G, Hirose Y, Mori T. Activation of endothelial nitric oxide synthase by cilostazol via a cAMP/protein kinase A- and phosphatidylinositol 3-kinase/Akt-dependent mechanism. *Atherosclerosis*. 2006;189:350–357.
9. Hayashi T, Matsui-Hirai H, Miyazaki-Akita A, Fukatsu A, Funami J, Ding QF, Kamalanathan S, Hattori Y, Ignarro LJ, Iguchi A. Endothelial cellular senescence is inhibited by nitric oxide: implications in atherosclerosis associated with menopause and diabetes. *Proc Natl Acad Sci USA*. 2006;103:17018–17023.
10. Vasa M, Breitschopf K, Zeiher AM, Dimmeler S. Nitric oxide activates telomerase and delays endothelial cell senescence. *Circ Res*. 2000;87:540–542.
11. Braunstein M, Rose AB, Holmes SG, Allis CD, Broach JR. Transcriptional silencing in yeast is associated with reduced nucleosome acetylation. *Genes Dev*. 1993;7:592–604.
12. Vaziri H, Dessain SK, Ng Eaton E, Imai SI, Frye RA, Pandita TK, Guarente L, Weinberg RA. hSIR2 (SIRT1) functions as an NAD-dependent p53 deacetylase. *Cell*. 2001;107:149–159.
13. Langley E, Pearson M, Faretta M, Bauer UM, Frye RA, Minucci S, Pelicci PG, Kouzarides T. Human SIR2 deacetylates p53 and antagonizes PML/p53-induced cellular senescence. *EMBO J*. 2002;21:2383–2396.
14. Picard F, Kurtev M, Chung N, Topark-Ngarm A, Senawong T, Machado De Oliveira R, Leid M, McBurney MW, Guarente L. Sirt1 promotes fat mobilization in white adipocytes by repressing PPAR-gamma. *Nature*. 2004;429:771–776.
15. Nisoli E, Tonello C, Cardile A, Cozzi V, Bracale R, Tedesco L, Falcone S, Valerio A, Cantoni O, Clementi E, Moncada S, Carruba MO. Calorie restriction promotes mitochondrial biogenesis by inducing the expression of eNOS. *Science*. 2005;310:314–317.
16. Maciag T, Hoover GA, Stemerman MB, Weinstein R. Serial propagation of human endothelial cells in vitro. *J Cell Biol*. 1981;91:420–426.
17. Shi Y, Man RY, Vanhoutte PM. Two isoforms of cyclooxygenase contribute to augmented endothelium-dependent contractions in femoral arteries of 1-year-old rats. *Acta Pharmacol Sin*. 2008;29:185–192.
18. Frew JE, Jones P, Scoles G. Spectrophotometric determination of hydrogen peroxide and organic hydroperoxides at low concentrations in aqueous solution. *Analytica chemica acta*. 1983;155:139–150.
19. Yokoi T, Fukuo K, Yasuda O, Hotta M, Miyazaki J, Takemura Y, Kawamoto H, IchijoH, Ogihara T. Apoptosis signal-regulating kinase 1 mediates cellular senescence induced by high glucose in endothelial cells. *Diabetes*. 2006;55:1660–1665.
20. Akiyama H, Kudo S, Shimizu T. The absorption, distribution and excretion of a new antithrombotic and vasodilating agent, cilostazol, in rat, rabbit, dog and man. *Arzneimittelforschung*. 1985;35:1124–1132.
21. Ota H, Akishita M, Eto M, Iijima K, Kaneki M, Ouchi Y. Sirt1 modulates premature senescence-like phenotype in human endothelial cells. *J Mol Cell Cardiol*. 2007;43:571–579.
22. Albrecht EW, Stegeman CA, Heeringa P, Henning RH, van Goor H. Protective role of endothelial nitric oxide synthase. *J Pathol*. 2003;199:8–17.
23. Sato I, Morita I, Kaji K, Ikeda M, Nagao M, Murota S. Reduction of nitric oxide producing activity associated with in vitro aging in cultured human umbilical vein endothelial cell. *Biochem Biophys Res Commun*. 1993;195:1070–1076.
24. Takase H, Hashimoto A, Okutsu R, Hirose Y, Ito H, Imaizumi T, Miyakoda G, Mori T. Anti-atherosclerotic effect of cilostazol in apolipoprotein-E knockout mice. *Arzneimittelforschung*. 2007;57:185–191.
25. Nakamura T, Houchi H, Minami A, Sakamoto S, Tsuchiya K, Niwa Y, Minakuchi K, Nakaya Y. Endothelium-dependent relaxation by cilostazol, a phosphodiesteras III inhibitor, on rat thoracic aorta. *Life Sci*. 2001;69:1709–1715.
26. Watanabe K, Ikeda S, Komatsu J, Inaba S, Suzuki J, Sueda S, Funada J, Kitakaze M, Sekiya M. Effect of cilostazol on vasomotor reactivity in patients with vasospastic angina pectoris. *Am J Cardiol*. 2003;92:21–25.

Geriatr Gerontol Int 2008; 8: 93–100

ORIGINAL ARTICLE: EPIDEMIOLOGY, CLINICAL PRACTICE AND HEALTH

White matter lesions as a feature of cognitive impairment, low vitality and other symptoms of geriatric syndrome in the elderly

Kazuki Sonohara,[1] Koichi Kozaki,[1] Masahiro Akishita,[2] Kumiko Nagai,[1] Hiroshi Hasegawa,[1] Masafumi Kuzuya,[3] Koutaro Yokote[4] and Kenji Toba[1]

[1]Department of Geriatric Medicine, Kyorin University School of Medicine, Mitaka, [2]Department of Geriatric Medicine, University of Tokyo Graduate School of Medicine, Tokyo, [3]Department of Geriatrics, Nagoya University Graduate School of Medicine, Nagoya, and [4]Department of Clinical Cell Biology and Medicine, Chiba University Graduate School of Medicine, Chiba, Japan

Aim: White matter lesions (WML) are common findings on magnetic resonance imaging (MRI) in elderly persons. In this study, we analyzed the relation of WML with global cognitive function, depression, vitality/volition, and 19 symptoms of geriatric syndrome in Japanese elderly patients who attended three university geriatric outpatient clinics.

Methods: Two hundred and eighty-six subjects (103 men and 183 women; mean ± standard deviation age, 74.5 ± 7.8 years) were included in this study. MRI scans were performed for the diagnosis of WML, and the severity of periventricular and deep white matter hyperintensities (PVH and DWMH) was rated semiquantitatively. Concurrently, all subjects underwent tests of cognitive function, depressive state and vitality, and were examined for 19 symptoms of geriatric syndrome.

Results: The study subjects showed cognitive decline, depression and low vitality, all to a mild extent. Univariate linear regression analysis showed a negative correlation between the severity of WML and cognitive function or vitality. Multiple logistic analysis revealed that the severity of WML was a significant determinant of cognitive impairment and low vitality, after adjustment for confounding factors such as age, sex and concomitant diseases. PVH and/or DWMH score was significantly greater in subjects who exhibited 13 out of 19 symptoms of geriatric syndrome. Logistic regression analysis indicated that WML were associated with psychological disorders, gait disturbance, urinary problems and parkinsonism.

Conclusion: WML were associated with various symptoms of functional decline in older persons. Evaluating WML in relation to functional decline would be important for preventing disability in elderly people.

Keywords: deep white matter hyperintensity, geriatric syndrome, periventricular hyperintensity, white matter lesion.

Accepted for publication 10 December 2007.

Correspondence: Assistant Professor Koichi Kozaki MD, Department of Geriatric Medicine, Kyorin University School of Medicine, 6-20-2 Shinkawa, Mitaka, Tokyo 181-8611, Japan. Email: kozaki-tky@umin.ac.jp

doi: 10.1111/j.1447-0594.2008.00454.x

Introduction

Brain magnetic resonance imaging (MRI) has markedly enhanced the chance of detecting characteristic hyperintense signals in the periventricular and subcortical areas on T2-weighted images, even in asymptomatic older persons.[1] These lesions are known as white matter lesions (WML), leukoaraiosis or white matter (periventricular and subcortical) hyperintensities.[2–4] WML, which accompany symptoms of gait abnormalities,[5–7] urinary symptoms[5,8,9] and cognitive impairment,[4,10,11] are reported to be associated with aging,[12–14] hypertension,[14] diabetes[15] and atherosclerosis.[5] There is poor understanding of the pathogenesis of the lesions, and it remains unknown whether WML are mere innocuous radiological changes that appear as a result of the aging process,[2,3,10] or whether they are one of the causal factors of the functional decline in elderly people.

Geriatric syndrome is a group of symptoms that are related to daily life, and the comorbidity triggers the loss of independence of elderly persons. Hence, evaluation of geriatric syndrome is important for the physical and mental care of the elderly. To address the pathological significance of WML in the global cognitive and psychological functions, and in geriatric syndrome in representative Japanese elderly subjects, we organized a group of geriatric outpatient clinics, and investigated the clinical manifestations of WML in those patients. Especially, we analyzed the relation of WML with global cognitive function, depressive state, vitality/volition and 19 symptoms of geriatric syndrome.

Methods

Subjects

This was a multicenter study performed at three different university geriatric outpatient clinics in Japan under the organization of a Longevity Science Research Grant from the Ministry of Health, Labor and Welfare of Japan (H15-Choju-013). Two hundred and eighty-six consecutive subjects (103 men and 183 women; mean ± standard deviation [SD] age, 74.5 ± 7.8 years) were included in this study: 187 at Kyorin University Hospital, 74 at Chiba University Hospital, and 25 at Nagoya University Hospital, from January 2004 to January 2005.

The diagnosis of dementia was made according to the Diagnostic and Statistical Manual of Mental Disorders, Fourth Edition (DSM-IV). The definition of hypertension was systolic blood pressure (BP) of more than 140 mmHg or diastolic BP of more than 90 mmHg, or receiving antihypertensive drugs. The definition of diabetes was glycosylated hemoglobin A1c of more than 6.5%, or receiving antidiabetic drugs. The definition of hyperlipidemia was total cholesterol of more than 5.72 mmol/L, triglyceride of more than 1.70 mmol/L, or receiving antihyperlipidemic drugs.

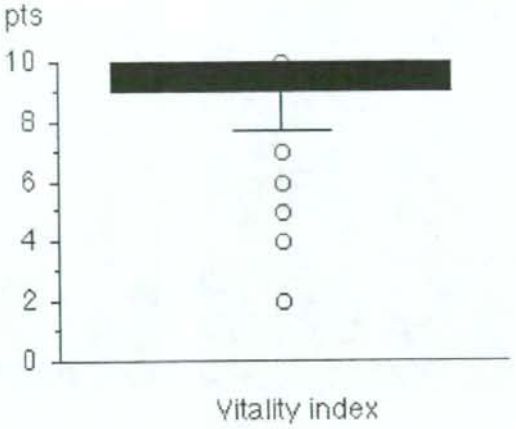

Figure 1 Distribution of vitality index. All subjects underwent assessment of vitality index as a measure of vitality related to activities of daily living (waking pattern, communication, feeding, getting on and off the toilet, rehabilitation and other activities; 2 points each; range, 0–10).

All subjects underwent the following assessment of global cognitive and psychological function. Cognitive function was evaluated by Mini-Mental State Examination (MMSE).[16] In this examination, we focused on calculation (serial subtraction of 7 from 100) to evaluate attention and working memory (part of the frontal lobe function). We also performed verbal fluency or word recollection test by asking the subjects to name as many vegetables as possible, which is also indicative of the frontal lobe function. Depression was evaluated by the 15-item Geriatric Depression Scale (GDS-15), which consists of 15 dichotomous questions for screening depressive symptoms in elderly subjects (range, 0–15).[17] Vitality index was used to measure vitality or volition in daily life (waking pattern, communication, feeding, getting on and off the toilet, rehabilitation and other activities; 2 points each; range, 0–10).[18] A full score can be maintained until one is severely disabled in cognition or function. The distribution of vitality index in the subjects of this study is shown in Figure 1.

We examined symptoms of geriatric syndrome: 19 dichotomous questions about hallucinations, delusions, insomnia, vertigo, paralysis, numbness, gait disturbance, tripping, falls, pollakiuria, urinary incontinence, constipation, decreased appetite, weight loss, apathy, speech impairment, swallowing difficulty, tremor and muscle stiffness.

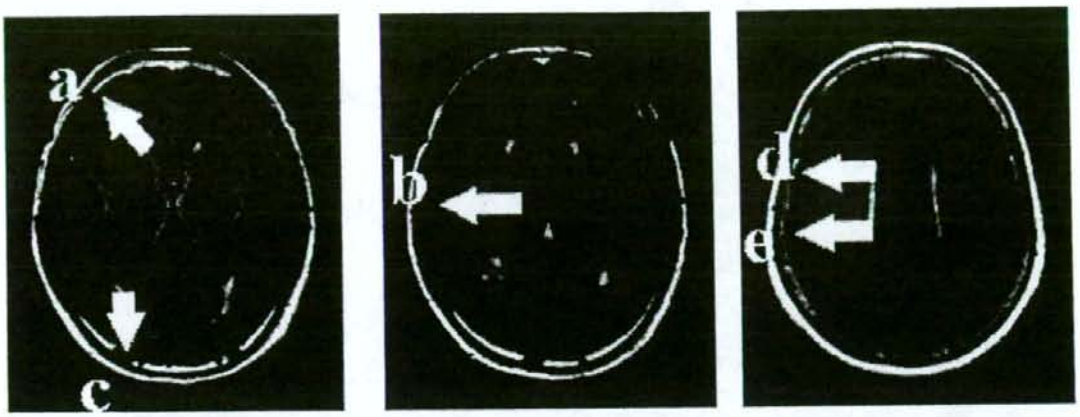

Figure 2 Evaluation of periventricular hyperintensity (PVH). PVH were evaluated in six regions in three slices: (a) adjacent to the frontal horns, (b) lateral ventricular body, (c) occipital horns, (d) frontal central semiovale in the parietal region and (e) occipital centrum semiovale in the parietal region in both hemispheres. Each area was rated as five grades according to the method of Junque *et al.*: (0) no hyperintensities; (1) <25% of the brain area; (2) 25–50%; (3) 50–75%; and (4) >75%.[11] The sum of all grades in the six regions was defined as the PVH score (range, 0–24).

Magnetic resonance imaging

Magnetic resonance imaging scans were performed for the diagnosis of WML and cerebral infarction on 1.5-T scanners (Toshiba, Nasu, Japan). T1-weighted images (repetition time [TR], 496 ms; echo time [TE], 12 ms), T2-weighted images (TR, 4280 ms; TE, 105 ms), and fluid-attenuated inversion-recovery (FLAIR)-weighted images (TR, 8000 ms; TE, 105 ms; 5-mm slice thickness) were obtained in the axial plane. MRI images were examined to differentiate between WML, characterized by isointense signals on T1-weighted images and hyperintense signals on T2-weighted and FLAIR images, and cerebral infarction, characterized by hypointense signals on T1-weighted images and hyperintense signals on T2-weighted and FLAIR images.

White matter lesions were classified as periventricular hyperintensities (PVH), which adjoined the lateral ventricle, and deep white matter hyperintensities (DWMH), located in the deep white matter apart from the lateral ventricles.

Periventricular and deep white matter hyperintensity scores

Periventricular hyperintensities were evaluated in six regions in three slices: adjacent to the frontal horns, lateral ventricular body, occipital horns, frontal central semiovale in the parietal region, and occipital centrum semiovale in the parietal region in both hemispheres (Fig. 2). Each area was rated as five grades according to the systematic quantification method developed by Junque *et al.*: (0) no hyperintensities; (1) less than 25% of the brain area; (2) 25–50%; (3) 50–75%; and (4) more than 75%.[11] The sum of all grades in the six regions was defined as the PVH score (range, 0–24).

Deep white matter hyperintensities were evaluated in the frontal, temporal, parietal and occipital lobes, and in the basal ganglia in both hemispheres (Fig. 3). Each lesion was rated as three grades according to the diameter by the study of de Groot *et al.*: (1) 1–3 mm; (2) 3–10 mm; and (3) more than 10 mm. The sum of all grades in five regions in both hemispheres was defined as the DWMH score.[4] Analysis was performed assuming that the white matter scores of PVH and DWMH were quantitative interval scales.

Statistical analysis

The relationship between two continuous variables such as MMSE, GDS-15 or vitality index, and WML (PVH or DWMH) score was analyzed by univariate linear regression analysis, and the correlation was analyzed by means of Pearson's simple correlation coefficients. Statistical significance was set at $P < 0.05$.

The relation of cognitive impairment or low vitality with PVH score or DWMH score was assessed by means of multivariate logistic regression analysis with adjustment for age, sex, hypertension, diabetes, hyperlipidemia and past history of cerebrovascular disease, of which all variables other than age were treated as categorical data. Cognitive impairment and low vitality were defined as an MMSE score of 23 or less[19] and a vitality index of 9 or less, respectively. Odds ratios and 95% confidence interval were calculated from the, coefficients and their standard errors.

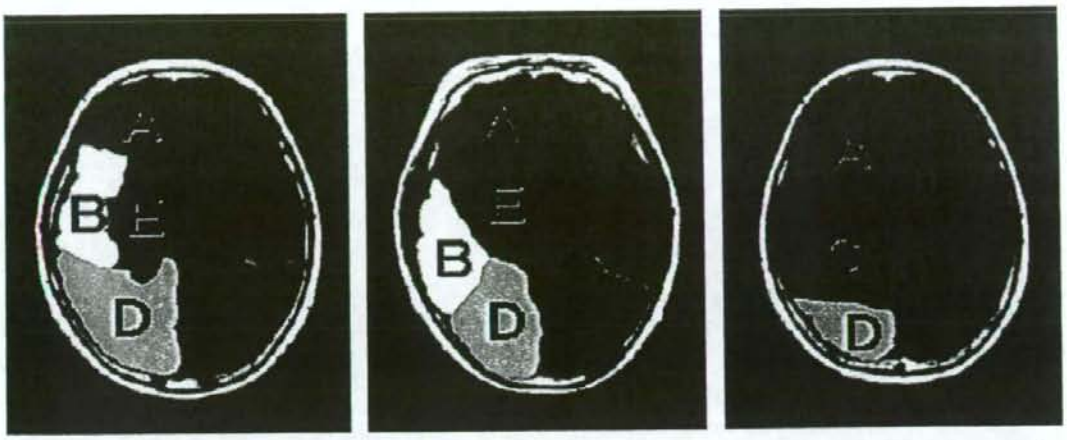

Figure 3 Evaluation of deep white matter hyperintensities (DWMH). DWMH were evaluated in the (A) frontal, (B) temporal, (C) parietal and (D) occipital lobes, and (E) in the basal ganglia in both hemispheres. Each lesion was rated as three grades according to diameter by the method of de Groot *et al.*: (1) 1–3 mm; (2) 3–10 mm; and (3) >10 mm.[4] The sum of all grades in five regions in both hemispheres was defined as the DWMH score.

Periventricular hyperintensity score or DWMH score was compared between subjects who did or did not exhibit each symptom of geriatric syndrome and analyzed by Student's *t*-test. When the difference was considered to be significant ($P < 0.05$), the difference was further assessed by means of multivariate logistic regression analysis with adjustment for age, sex, hypertension, diabetes, hyperlipidemia and past history of cerebrovascular disease.

Ethical considerations

This study was approved by the ethical committees of the institutes involved in this project. We explained this study clearly, and obtained written consent from all participants and their guardians (mainly family members). All the data were stored and analyzed carefully to preserve the subjects' anonymity and protect their privacy.

Results

Clinical data

The clinical characteristics of the study subjects are shown in Table 1. The mean age of subjects was 74.5 ± 7.8 years (mean ± SD), and subjects aged 65 or older comprised 88.1%. The mean body mass index was 21.8 ± 3.3 kg/m^2 and none of the subjects were obese. Of the subjects, 10.1% had experienced stroke or other cerebrovascular disease and 22.7% were smokers. Hypertension, diabetes and hyperlipidemia were present in 50.7%, 27.3% and 50.0% of the subjects, respectively.

White matter lesions

Periventricular hyperintensities and DWMH were observed in 77.7% and 96.7% of the total subjects, respectively. The mean score of PVH and DWMH was 5.5 ± 4.8 and 35.5 ± 39.8, respectively (Table 1). Pearson's correlation analysis showed a strong positive correlation between PVH score and DWHM score ($r = 0.56$, $P < 0.0001$). In relation to aging, a positive correlation was found between PVH score and age ($r = 0.34$, $P < 0.0001$), and between DWMH score and age ($r = 0.28$, $P < 0.0001$).

Cognitive and psychological assessment

The mean score of MMSE, GDS-15 and vitality index was 23.1 ± 5.3, 5.0 ± 3.5 and 9.4 ± 1.2 points, respectively, indicating that the subjects showed cognitive decline, depression and decreased vitality, all to a mild extent. Given that a score of 23 or below on MMSE is regarded as the presence of cognitive impairment,[19] 47.5% of the subjects fell into this category. The causes of cognitive impairment were Alzheimer disease (AD; 53.3%), vascular dementia (VaD; 16.4%), combined dementia of AD and VaD (9.0%) and other types of dementia (21.3%). Pearson's correlation analysis revealed a negative correlation between PVH score and MMSE, PVH score and vitality index, DWMH score and MMSE, and DWMH score and vitality index,

Table 1 Clinical characteristics of study subjects

	Prevalence ($n = 286$)	Mean ± standard deviation
Clinical characteristics		
Age (years)		74.5 ± 7.8
Women (%)	74.0	
Height (m)		1.55 ± 0.08
Bodyweight (kg)		52.4 ± 10.6
Body mass index (kg/m^2)		21.8 ± 3.3
Systolic blood pressure (mmHg)		135.3 ± 20.2
Diastolic blood pressure (mmHg)		76.3 ± 11.8
Prevalence of complications		
Hypertension (%)	50.7	
Diabetes (%)	27.3	
Hyperlipidemia (%)	50.0	
Past history of cerebrovascular disease (%)	10.1	
Smoking (%)	22.7	
Cognitive and psychological assessment		
Mini-Mental State Examination (0–30 points)		23.1 ± 5.3
Geriatric depression scale (0–15 points)		5.0 ± 3.5
Vitality index (0–10 points)		9.4 ± 1.2
White matter lesions		
Periventricular hyperintensities (points)	5.5 ± 4.8	
Deep white matter hyperintensities (points)	35.5 ± 39.8	

Table 2 Relationship between white matter lesions and global cognition (MMSE), depressive state (GDS-15) and vitality (vitality index)

	Linear regression PVH score	DWMH score
MMSE	−0.380**	−0.272**
GDS-15	0.022	−0.066
Vitality index	−0.432**	−0.184*

Univariate linear regression analysis: *$P < 0.01$, **$P < 0.0001$. DVMH, deep white matter hyperintensity; GDS-15, 15-item Geriatric Depression Scale; MMSE, Mini-Mental State Examination; PVH, periventricular hyperintensity.

respectively (Table 2). It was also found that calculation (serial subtraction of 7 from 100) was negatively correlated with PVH score ($r = -0.156$, $P = 0.04$, data not shown), and verbal fluency (naming as many vegetables as possible) was negatively correlated with PVH score ($r = -0.216$, $P < 0.01$, data not shown). On the other hand, no significant correlation was found between PVH score and GDS-15, or between DWMH score and GDS-15. Multiple logistic analysis revealed that PVH score and DWMH score remained significant determinants of cognitive impairment (MMSE, ≤23) and low vitality (vitality index, ≤9) after adjustment for age, sex, presence of hypertension, diabetes, hyperlipidemia and past history of cerebrovascular disease (Table 3).

One hundred and ninety subjects reported symptoms of geriatric syndrome. The frequency is shown in Table 4. Frequent symptoms (>20%) were tripping (32.1%), constipation (26.3%), gait disturbance (23.2%) and pollakiuria (22.1%). Student's *t*-test showed that PVH score was significantly greater in subjects who exhibited the following symptoms of geriatric syndrome: hallucinations, delusions, gait disturbance, tripping, falls, pollakiuria, urinary incontinence, weight loss, apathy, swallowing difficulty, tremor and muscle stiffness. Multiple logistic analysis revealed that PVH score remained a significant determinant of hallucinations, tripping, pollakiuria, urinary incontinence, weight loss, apathy and swallowing difficulty after adjustment for age, sex, presence of hypertension, diabetes, hyperlipidemia and past history of cerebrovascular disease (Table 5). By the same method, DWMH score was

Table 3 Periventricular hyperintensity and deep white matter hyperintensity scores as determinants of cognitive impairment and low vitality

	PVH score			DWMH score		
	OR	95% CI	*P*-value	OR	95% CI	*P*-value
Cognitive impairment	1.185	1.084–1.295	<0.001	1.010	1.001–1.021	<0.05
Low vitality	1.260	1.133–1.401	<0.0001	1.025	1.012–1.039	<0.001

Cognitive impairment and low vitality were defined as MMSE ≤23 and vitality index ≤9, respectively. Multiple logistic analysis was performed after adjustment for age, sex, hypertension, diabetes, hyperlipidemia, and past history of cerebrovascular disease, of which all variables other than age were treated as categorical data. CI, confidence interval; DVMH, deep white matter hyperintensity; OR, odds ratio; PVH, periventricular hyperintensity.

significantly greater in subjects who exhibited the following symptoms of geriatric syndrome: hallucinations, delusions, gait disturbance, tripping, falls, pollakiuria, urinary incontinence and constipation. Multiple logistic analysis revealed that DWMH score remained a significant determinant of hallucinations, delusions, tripping, urinary incontinence and constipation after adjustment for age, sex, presence of hypertension, diabetes, hyperlipidemia and past history of cerebrovascular disease (Table 6).

Discussion

Elderly persons are affected by multiple chronic diseases. Once they are affected by serious illness, full recovery cannot be expected with medical treatment, because elderly patients are often trapped in a vicious circle of illness and poor quality of life (QOL). This is the reason why care and welfare contribute to the total well-being of the elderly. Physicians need to pay great attention to improving QOL as well as treating illness. Thus, it is important to comprehend the whole picture of their life by means of comprehensive geriatric assessment, which evaluates multiple aspects of an elderly person's life, such as activities of daily living, cognition, mood, vitality, communication and social environment.

The present study confirmed a negative correlation between the severity of WML and MMSE score. Multivariate analysis showed that the presence of WML was a significant risk factor for cognitive impairment, even after adjustment for confounding factors of age, sex, hypertension, diabetes, hyperlipidemia and past history of cerebrovascular disease. The mechanism and the size and location of WML that impair cognitive function are not yet clear. However, from previous studies, it seems convincing that a reduction of blood flow in the frontal lobe plays an important role in cognitive impairment in elderly people who exhibit WML.[20,21] Clinical manifestations of WML include attention deficit and a decline in information-processing ability.[4,13,22] Junque *et al.* reported the reappearance of primitive reflexes, one of the symptoms of frontal lobe dysfunction, in patients with WML.[11] In this study, patients with PVH showed attention deficit (incapability of calculation) and verbal inarticulacy (naming less vegetables), implying the impairment of frontal lobe function. WML, as reported previously,[6,23] were negatively correlated with vitality. Multiple logistic regression analysis, using potential risk factors including advanced age as confounding variables, found that the presence of WML was an independent risk factor for low vitality. Additionally, a relation between PVH score and apathy, a significant symptom of geriatric syndrome, was also found. From previous studies showing the importance of frontal lobe function in vitality,[24–26] we assume that blood flow reduction in the frontal lobe may account for the apathy and low vitality in patients with WML. More precisely, WML disrupting the frontal-subcortical circuit may result in dysfunction in the anterior cingulate and dorsolateral prefrontal circuits, thereby leading to apathy and decreased vitality.[5,6,20] Increase in PVH score or DWMH score was not apparently correlated with depression, probably because depression is associated with many factors such as aging, female sex, hyperlipidemia and medication.[27–29] The subjects in this study were mostly elderly (88.1%) and female (74.0%). We assume that these confounding conditions made it difficult to prove a true relation between WML and depression. From analysis of the association of WML with geriatric syndrome, it appears that WML have a relation to psychiatric symptoms (hallucinations and delusions), gait abnormalities (gait disturbance, tripping and falls), urinary symptoms (pollakiuria and urinary incontinence) and possibly with parkinsonism (swallowing difficulty, tremor and muscle stiffness). It was reported that WML were related to gait abnormalities,[5–7] presumably caused by disruption of the frontal-subcortical circuit.[30] Some other studies suggested that parkinsonism is also a contributing factor to gait disturbance in patients with WML.[6,31] Interestingly, we found that both gait abnormalities and symptoms of parkinsonism were associated with WML.

The present study confirmed an association between WML and voiding dysfunction (pollakiuria and incontinence). It was reported that urinary dysfunction was derived from damage to the frontal-subcortical

Table 4 Comparison of periventricular hyperintensity and deep white matter hyperintensity scores between subjects who did or did not exhibit each symptom of geriatric syndrome

Geriatric syndrome	Prevalence (%)	PVH score Symptom Present	Absent	*P*-value	DWMH score Symptom Present	Absent	*P*-value
Hallucination	6.8	**8.5 ± 5.9**	**4.4 ± 4.7**	**<0.01**	**59.8 ± 43.9**	**28.6 ± 35.4**	**<0.01**
Delusion	9.5	**7.6 ± 5.2**	**4.4 ± 4.8**	**0.01**	**56.1 ± 37.6**	**28.2 ± 35.9**	**<0.01**
Insomnia	18.9	4.2 ± 3.6	4.7 ± 4.9	0.56	31.4 ± 36.0	31.3 ± 37.6	0.98
Vertigo	18.9	6.1 ± 6.5	4.4 ± 4.4	0.06	33.4 ± 38.1	30.7 ± 37.0	0.70
Paralysis	2.1	8.5 ± 4.8	4.6 ± 4.9	0.12	59.5 ± 47.2	30.1 ± 36.3	0.11
Numbness	16.6	5.1 ± 4.6	4.6 ± 4.8	0.62	34.6 ± 40.0	29.9 ± 36.0	0.52
Gait disturbance	23.2	**6.7 ± 5.1**	**4.2 ± 4.7**	**<0.01**	**43.3 ± 41.7**	**27.5 ± 34.9**	**0.01**
Tripping	32.1	**6.4 ± 4.5**	**3.9 ± 4.9**	**<0.01**	**42.1 ± 43.7**	**25.9 ± 32.4**	**<0.01**
Falls	17.9	**6.6 ± 4.9**	**4.3 ± 4.8**	**0.01**	**45.8 ± 43.1**	**28.0 ± 35.0**	**0.01**
Pollakiuria	22.1	**8.0 ± 5.8**	**3.8 ± 4.2**	**<0.01**	**41.5 ± 41.0**	**41.5 ± 41.0**	**0.04**
Urinary incontinence	13.8	**7.5 ± 5.1**	**4.3 ± 4.8**	**<0.01**	**52.4 ± 44.9**	**52.4 ± 44.9**	**<0.01**
Constipation	26.3	5.8 ± 4.3	4.4 ± 5.1	0.08	**44.5 ± 45.1**	**44.5 ± 45.1**	**<0.01**
Decreased appetite	14.7	6.1 ± 4.4	4.5 ± 5.0	0.12	42.1 ± 42.6	42.1 ± 42.6	0.11
Weight loss	14.2	**6.9 ± 4.1**	**4.4 ± 5.0**	**0.01**	40.7 ± 41.3	40.7 ± 41.3	0.15
Apathy	7.6	**7.4 ± 3.6**	**4.4 ± 5.0**	**0.03**	30.7 ± 28.1	30.7 ± 28.1	0.97
Speech impairment	2.7	5.6 ± 5.2	4.5 ± 4.7	0.62	35.3 ± 48.0	35.3 ± 48.0	0.80
Swallowing difficulty	14.7	**12.2 ± 4.4**	**4.5 ± 4.8**	**<0.01**	44.6 ± 34.6	44.6 ± 34.6	0.40
Tremor	5.3	**9.1 ± 6.5**	**4.4 ± 4.7**	**<0.01**	45.0 ± 38.1	45.0 ± 38.1	0.24
Muscle stiffness	3.2	**9.2 ± 4.8**	**4.5 ± 4.9**	**0.02**	48.7 ± 43.4	48.7 ± 43.4	0.23

PVH and DWMH score are shown as mean ± SD. Boldface values are statistically significant ($P < 0.05$ by Student's *t*-test). DVMH, deep white matter hyperintensity; PVH, periventricular hyperintensity.

Table 5 Periventricular hyperintensity score as determinant of geriatric syndrome

	OR	*P*-value	95% CI
Hallucination	1.12	0.043	1.004–1.248
Tripping	1.11	0.005	1.032–1.194
Pollakiuria	1.17	0.001	1.067–1.278
Urinary incontinence	1.11	0.022	1.015–1.207
Weight loss	1.14	0.007	1.036–1.246
Apathy	1.14	0.027	1.015–1.276
Swallowing difficulty	1.35	0.019	1.050–1.741

Multiple logistic analysis was performed to analyze each symptom of geriatric syndrome, with adjustment for age, sex, hypertension, diabetes, hyperlipidemia and past history of cerebrovascular disease, of which all variables other than age were treated as categorical data. CI, confidence interval; OR, odds ratio.

Table 6 Deep white matter hyperintensity score as determinant of geriatric syndrome

	OR	*P*-value	95% CI
Hallucination	1.017	0.020	1.003–1.032
Delusion	1.016	0.024	1.002–1.030
Tripping	1.011	0.020	1.002–1.020
Urinary incontinence	1.016	0.008	1.004–1.028
Constipation	1.011	0.025	1.001–1.021

Multiple logistic analysis was performed to analyze each symptom of geriatric syndrome, with adjustment for age, sex, hypertension, diabetes, hyperlipidemia and past history of cerebrovascular disease, of which all variables other than age were treated as categorical data. CI, confidence interval; OR, odds ratio.

circuit.[5,20] In relation to the symptoms of parkinsonism (swallowing difficulty, tremor and muscle stiffness), this association was previously explained by dysfunction of the frontal-subcortical circuit.[6,31] The importance of this lesion was also suggested by a study showing that swallowing difficulty occurs with dysfunction of internuncial neurons that link the brainstem to the cerebral cortex.[32]

Considering the cause of manifestation of geriatric syndrome in patients with WML, it appears that damage to associative pathways in the frontal and subcortical regions due to ischemic hypoperfusion is an important mechanism.[5,20,21] It is necessary to localize the responsible connecting pathway for each symptom by a sophisticated approach in the future.

In conclusion, we showed that WML were associated with cognitive impairment, low vitality and geriatric syndrome of psychological disorders, gait disturbance,

urinary problems and parkinsonism. Evaluating WML in relation to geriatric syndrome and building a preventive measure against WML is an important future task for maintaining the independence of elderly people.

Acknowledgments

This study was supported by a Longevity Science Research Grant from the Ministry of Health, Labor and Welfare of Japan (H15-Choju-013) and by Mitsui Sumitomo Insurance Welfare Foundation (2004, 2006), and by the Japan Health Foundation. We thank Yukiko Yamada and Ayako Machida for their technical assistance.

References

1 Breteler MM, van Swieten JC, Bots ML *et al.* Cerebral white matter lesions, vascular risk factors, and cognitive function in a population-based study: the Rotterdam Study. *Neurology* 1994; **44**: 1246–1252.
2 Hachinski VC, Potter P, Merskey H. Leuko-araiosis. *Arch Neurol* 1987; **44**: 21–23.
3 Hunt AL, Orrison WW, Yeo RA *et al.* Clinical significance of MRI white matter lesions in the elderly. *Neurology* 1989; **39**: 1470–1474.
4 de Groot JC, de Leeuw FE, Oudkerk M *et al.* Cerebral white matter lesions and cognitive function: the Rotterdam Scan Study. *Ann Neurol* 2000; **47**: 145–151.
5 Kuo HK, Lipsitz LA. Cerebral white matter changes and geriatric syndromes: is there a link? *J Gerontol A Biol Sci Med Sci* 2004; **59**: 818–826.
6 Starkstein SE, Sabe L, Vazquez S *et al.* Neuropsychological, psychiatric, and cerebral perfusion correlates of leuko-araiosis in Alzheimer's disease. *J Neurol Neurosurg Psychiatry* 1997; **63**: 66–73.
7 Baloh RW, Ying SH, Jacobson KM. A longitudinal study of gait and balance dysfunction in normal older people. *Arch Neurol* 2003; **60**: 835–839.
8 Sakakibara R, Hattori T, Uchiyama T, Yamanishi T. Urinary function in elderly people with and without leukoaraiosis: relation to cognitive and gait function. *J Neurol Neurosurg Psychiatry* 1999; **67**: 658–660.
9 Tarvonen-Schroder S, Roytta M, Raiha I, Kurki T, Rajala T, Sourander L. Clinical features of leuko-araiosis. *J Neurol Neurosurg Psychiatry* 1996; **60**: 431–436.
10 Pantoni L, Garcia JH. The significance of cerebral white matter abnormalities 100 years after Binswanger's report. *Stroke* 1995; **26**: 1293–1301.
11 Junque C, Pujol J, Vendrell P *et al.* Leuko-araiosis on magnetic resonance imaging and speed of mental processing. *Arch Neurol* 1990; **47**: 151–156.
12 Fazekas F. Magnetic resonance signal abnormalities in asymptomatic individuals: their incidence and functional correlates. *Eur Neurol* 1989; **29**: 164–168.
13 Ylikoski R, Ylikoski A, Erkinjuntti T, Sulkava R, Raininko R, Tilvis R. White matter changes in healthy elderly persons correlate with attention and speed of mental processing. *Arch Neurol* 1993; **50**: 818–824.
14 Fu JH, Lu CZ, Hong Z, Dong Q, Luo Y, Wong KS. Extent of white matter lesions is related to acute subcortical infarcts and predicts further stroke risk in patients with first ever ischaemic stroke. *J Neurol Neurosurg Psychiatry* 2005; **76**: 793–796.
15 Taylor WD, MacFall JR, Provenzale JM *et al.* Serial MR imaging of volumes of hyperintense white matter lesions in elderly patients: correlation with vascular risk factors. *Am J Roentgenol* 2003; **181**: 571–576.
16 Folstein MF, Folstein SE, McHugh PR. "Mini-Mental State". A practical method for grading the cognitive state of patients for the clinician. *J Psychiat Res* 1975; **12**: 189–198.
17 Sheikh JI, Yesavage JA. Geriatric Depression Scale (GDS): recent evidence and development of a short version. *Clin Gerontol* 1986; **56**: 165–173.
18 Toba K, Nakai R, Akishita M *et al.* Vitality index as a useful tool to assess elderly with dementia. *Geriatr Gerontol Int* 2002; **2**: 23–29.
19 Cullen B, Fahy S, Cunningham CJ *et al.* Screening for dementia in an Irish community sample using MMSE: a comparison of norm-adjusted versus fixed cut-points. *Int J Geriatr Psychiatry* 2005; **20**: 371–376.
20 Pugh KG, Lipsitz LA. The microvascular frontal–subcortical syndrome of aging. *Neurobiol Aging* 2002; **23**: 421–431.
21 Yao H, Sadoshima S, Kuwabara Y, Ichiya Y, Fujishima M. Cerebral blood flow and oxygen metabolism in patients with vascular dementia of the Binswanger type. *Stroke* 1990; **21**: 1694–1699.
22 Burton EJ, Kenny RA, O'Brien J *et al.* White matter hyperintensities are associated with impairment of memory, attention, and global cognitive performance in older stroke patients. *Stroke* 2004; **35**: 1270–1275.
23 Thomas P, Hazif-Thomas C, Saccardy F, Vandermarq P. Loss of motivation and frontal dysfunction. Role of the white matter change. *Encephale* 2004; **30**: 52–59.
24 Okada K, Kobayashi S, Yamagata S, Takahashi K, Yamaguchi S. Poststroke apathy and regional cerebral blood flow. *Stroke* 1997; **28**: 2437–2441.
25 Craig AH, Cummings JL, Fairbanks L *et al.* Cerebral blood flow correlates of apathy in Alzheimer disease. *Arch Neurol* 1996; **53**: 1116–1120.
26 Benoit M, Koulibaly PM, Migneco O, Darcourt J, Pringuey DJ, Robert PH. Brain perfusion in Alzheimer's disease with and without apathy: a SPECT study with statistical parametric mapping analysis. *Psychiatry Res* 2002; **15**: 103–111.
27 Stordal E, Mykletun A, Dahl AA. The association between age and depression in the general population: a multivariate examination. *Acta Psychiatr Scand* 2003; **107**: 132–141.
28 Terao T, Iwata N, Kanazawa K *et al.* Low serum cholesterol levels and depressive state in human dock visitors. *Acta Psychiatr Scand* 2000; **101**: 231–234.
29 Noble RE. Depression in women. *Metabolism* 2005; **54**: 49–52.
30 Hennerici MG, Oster M, Cohen S, Schwartz A, Motsch L, Daffertshofer M. Are gait disturbances and white matter degeneration early indicators of vascular dementia? *Dementia* 1994; **5**: 197–202.
31 Piccini P, Pavese N, Canapicchi R *et al.* White matter hyperintensities in Parkinson's disease. Clinical correlations. *Arch Neurol* 1995; **52**: 191–194.
32 Daniels SK, Foundas AL. Lesion localization in acute stroke patients with risk of aspiration. *J Neuroimaging* 1999; **9**: 91–98.

0013-7227/08/$15.00/0
Printed in U.S.A.

Endocrinology 149(4):1646–1653

doi: 10.1210/en.2007-1021

Adiponectin Antagonizes Stimulatory Effect of Tumor Necrosis Factor-α on Vascular Smooth Muscle Cell Calcification: Regulation of Growth Arrest-Specific Gene 6-Mediated Survival Pathway by Adenosine 5′-Monophosphate-Activated Protein Kinase

Bo-Kyung Son, Masahiro Akishita, Katsuya Iijima, Koichi Kozaki, Koji Maemura, Masato Eto, and Yasuyoshi Ouchi

Department of Geriatric Medicine (B.-K.S., M.A., K.I., M.E., Y.O.), the Department of Cardiovascular Medicine (K.M.), Graduate School of Medicine, The University of Tokyo, Tokyo 113-8655, Japan; and the Department of Geriatric Medicine (K.K.), School of Medicine, The University of Kyorin, Tokyo 181-8611, Japan

Adiponectin exhibits diverse protective effects against atherogenesis and antagonizes many effects of TNFα. Here, we investigated the effect of adiponectin and TNFα on vascular calcification, a critical event in the development and progression of vascular disease. In human aortic smooth muscle cells (HASMC), TNFα augmented inorganic phosphate (Pi)-induced calcification, whereas adiponectin significantly suppressed it and abolished the stimulatory effect of TNFα in a concentration-dependent manner. Similarly, adiponectin ameliorated the accelerating effect of TNFα on Pi-induced apoptosis, the essential process of HASMC calcification. Furthermore, these effects of TNFα and adiponectin were associated with AMP-activated protein kinase (AMPK)-dependent growth arrest-specific gene 6 (Gas6) expression and Akt signaling. The AMPK activator, 5-aminoimidazole-4-carboxamide ribonucleoside (AICAR), induced phosphorylation of AMPK and significantly inhibited Pi-induced calcification in HASMC. Conversely, pharmacological inhibition of AMPK by compound C blocked both AMPK activation and the inhibitory effect of adiponectin on calcification, providing evidence that AMPK plays a regulatory role in vascular calcification. Reporter assay revealed that adiponectin restored Gas6 promoter activity decreased by TNFα, and the effect of adiponectin was abrogated by compound C. These results demonstrate that adiponectin antagonizes the stimulatory effect of TNFα on vascular calcification by restoration of the AMPK-dependent Gas6-mediated survival pathway. (*Endocrinology* 149: 1646–1653, 2008)

VASCULAR CALCIFICATION is often encountered in advanced atherosclerotic lesions and is a common consequence of aging (1, 2). Calcification of the coronary arteries has been shown to be positively correlated with atherosclerotic plaque burden, increased risk of myocardial infarction, and plaque instability (3–5). We recently demonstrated that apoptosis plays an important role in inorganic phosphate (Pi)-induced vascular smooth muscle cell (VSMC) calcification (6). This type of calcification is dependent on down-regulation of the growth arrest-specific gene 6 (Gas6)-mediated survival pathway.

Adiponectin is an adipocyte-derived cytokine that exhibits protective properties in the heart and blood vessels (7–10). It accumulates in injured arteries from plasma and suppresses the endothelial inflammatory response (11) and VSMC proliferation (12). Furthermore, low plasma adiponectin levels are associated with progression of coronary artery calcification in type 1 diabetic and nondiabetic subjects, independent of other cardiovascular risk factors (13). Experimental studies have shown that adiponectin reduces TNFα production in response to various stresses, whereas TNFα attenuates adiponectin production, resulting in a reduction of plasma adiponectin levels (14–16). In addition to the inverse relationship between their expression, increasing evidence supports suppressive effects on each other's function (11, 17, 18). Given the importance of the reciprocal effects of TNFα and adiponectin, it is not clear whether both play a regulatory role in VSMC calcification.

Most of the beneficial actions of adiponectin are accounted for by the activation of AMP-activated protein kinase (AMPK) (19, 20). AMPK is a serine/threonine protein kinase that plays a key role in metabolic homeostasis in all eukaryotic cell types (21). Cardioprotective effects of adiponectin, including antiapoptotic actions, are also likely to be dependent on AMPK (19, 22, 23). However, the role of AMPK in the effect of adiponectin on VSMC calcification has not been addressed.

In the present study, we investigated whether adiponectin and TNFα modulate Pi-induced VSMC calcification by regulating apoptosis. We found that TNFα had a stimulatory effect, whereas adiponectin had an inhibitory effect on Pi-induced apoptosis and calcification in human aortic smooth muscle cells (HASMC). Furthermore, these actions were mediated by regulation of Gas6 at the transcription level via AMPK activation.

First Published Online January 3, 2008

Abbreviations: AICAR, 5-Aminoimidazole-4-carboxamide ribonucleoside; AMPK, AMP-activated protein kinase; Gas6, growth arrest-specific gene 6; HASMC, human aortic smooth muscle cells; Pi, inorganic phosphate; PP2C, protein phosphatase 2C; siRNA, small interfering RNA; TUNEL, terminal deoxynucleotidyl transferase-mediated dUTP nick end-labeling; VSMC, vascular smooth muscle cells.

Endocrinology is published monthly by The Endocrine Society (http://www.endo-society.org), the foremost professional society serving the endocrine community.

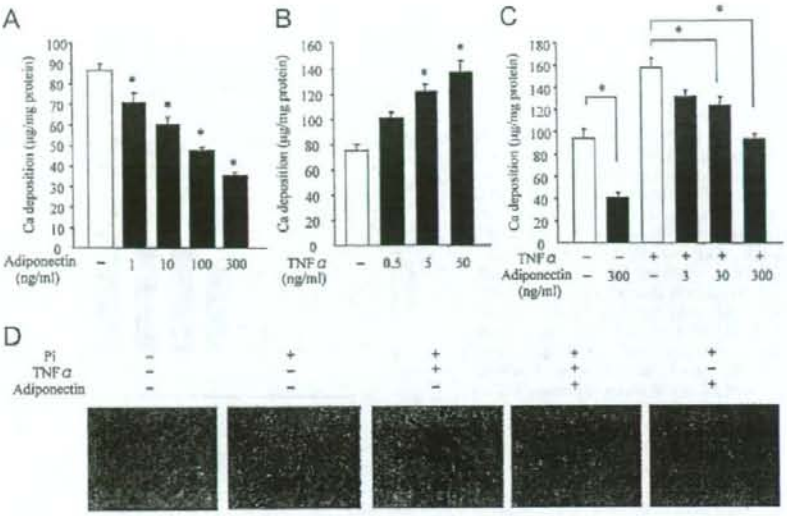

FIG. 1. Effect of adiponectin and TNFα on Pi-induced calcification. A and B, HASMC were cultured with the indicated concentrations of adiponectin (A) or TNFα (B) in calcification medium. They were added simultaneously when the medium was changed every 2 d. C, The effect of TNFα (20 ng/ml) and adiponectin with the indicated concentrations on Ca deposition was determined at 6 d. D, The effect of TNFα (20 ng/ml) and adiponectin (300 ng/ml) on Ca deposition was evaluated with von Kossa's staining at the light microscopic level. All values are presented as mean ± SE (n = 6). *, $P < 0.05$ by Bonferroni test. Each experiment was performed at least in triplicate for each condition.

Materials and Methods

Cell culture

HASMC were purchased from Clonetics Corp. (San Diego, CA). They were cultured in DMEM supplemented with 20% FBS, 100 U/ml penicillin, and 100 mg/ml streptomycin at 37 C in a humidified atmosphere with 5% CO_2. HASMC were used up to passage 8 for the experiments.

Induction and quantification of calcification

For Pi-induced calcification, Pi (a mixed solution of Na_2HPO_4 and NaH_2PO_4 whose pH was adjusted to 7.4) was added to serum-supplemented DMEM to a final concentration of 2.6 mM (calcification medium). Ca deposition was evaluated by the *o*-cresolphthalein complexone method (C-Test; WAKO, Osaka, Japan) and von Kossa's staining, as previously described (6, 24).

Determination of apoptosis

To examine the effect of TNFα (Sigma-Aldrich, St. Louis, MO) and adiponectin (R&D Systems, Minneapolis, MN) on Pi-induced apoptosis, they were added simultaneously when the medium was switched to the calcification medium. Apoptosis was detected by DNA fragmentation with a cell-death detection ELISA^{plus} kit (Roche, Manheim, Germany) and ter-

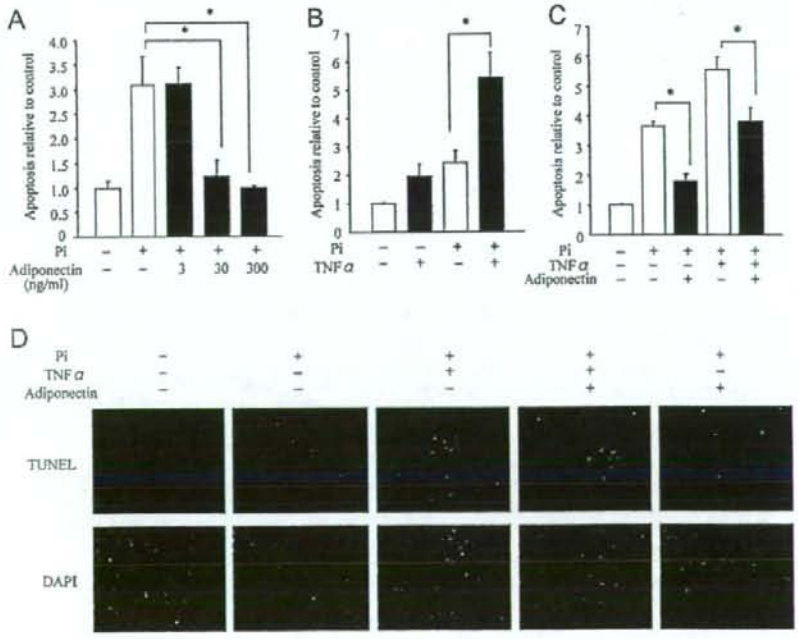

FIG. 2. Effect of adiponectin and TNFα on Pi-induced apoptosis. HASMC were cultured with the indicated concentrations of adiponectin for 6 d. Calcification medium was exchanged every 2 d. A, A quantitative index of apoptosis, determined by ELISA, is presented as the value relative to that without Pi treatment. B, HASMC were incubated with or without TNFα (20 ng/ml) in the absence or presence of 2.6 mM Pi for 6 d. C and D, On d 6, the effect of adiponectin (300 ng/ml) and TNFα (20 ng/ml) on apoptosis in calcification medium was determined by ELISA (C) and evaluated with TUNEL staining (D, *green*). Nuclei were counterstained with DAPI (*blue*). All values are presented as mean ± SE (n = 3). *, $P < 0.05$ by Bonferroni test. Each experiment was performed in triplicate for each condition.

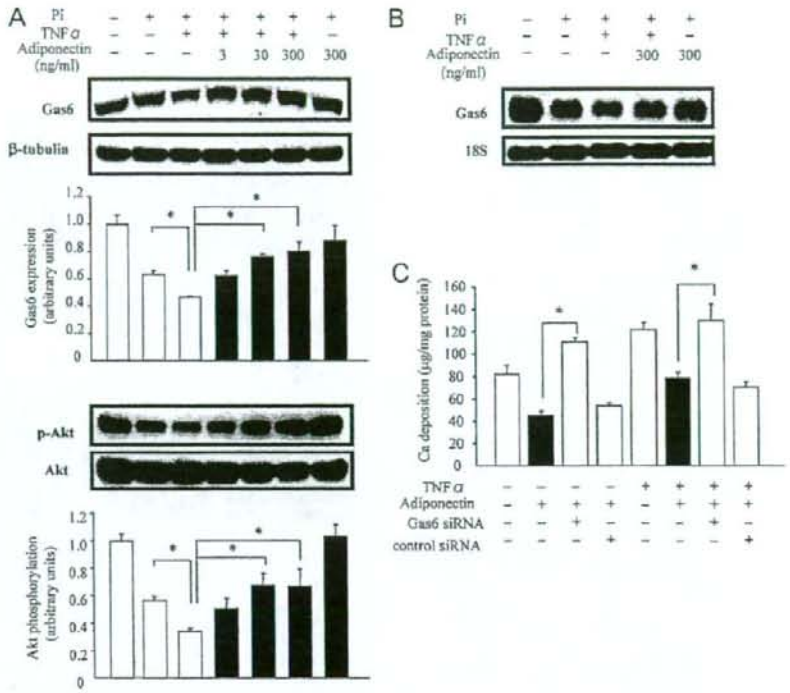

FIG. 3. Gas6 is the target of the effect of adiponectin and TNFα on Pi-induced calcification. HASMC were cultured with the indicated concentrations of adiponectin and TNFα (20 ng/ml). On d 6, cell lysates were collected and immunoblotted with antibodies that recognize Gas6, phospho-Akt (p-Akt), Akt, or β-tubulin. A, The untreated condition is the serum-supplemented status without Pi. B, Total RNA (5 μg) was harvested for Northern blot analysis after HASMC were incubated with adiponectin (300 ng/ml) and TNFα (20 ng/ml) for 6 d. When HASMC had reached 80–90% confluence, siRNA (100 nM) was transfected and then was transfected every 2 d with adiponectin (300 ng/ml) and TNFα (20 ng/ml) up to 6 d. C, Ca deposition was measured and normalized by cell protein content. All values are presented as mean ± SE (n = 3). *, $P < 0.05$ by Bonferroni test. Each experiment was performed in triplicate for each condition.

minal deoxynucleotidyl transferase-mediated dUTP nick end-labeling (TUNEL) assay with ApopTag Plus obtained from Chemicon International, Ltd. (Hampshire, UK), according to the manufacturer's instructions.

Generation of promoter reporter construct and luciferase activity assay

The 1925-bp Gas6 promoter (−1827/+99) corresponding to the Gas6 promoter sequences was generated by PCR from human genomic DNA with the appropriate sets of primers (6). These inserts were cloned into a pGL3 basic vector (Promega, Charbonnières, France) by standard molecular biological techniques. The construct was verified by sequencing. HASMC were transiently transfected in 12-well plates with 0.8 μg plasmid DNA and lipofectamine 2000 (Invitrogen Corp., Paisley, UK) according to the procedure recommended by the manufacturer. Cells were treated with TNFα, adiponectin, and compound C at 24 h after transfection, followed by incubation for an additional 44 h. Firefly luciferase activity was determined using a luciferase assay system (Promega) and normalized by total cell protein.

Preparation of small interfering RNA (siRNA) targeting Gas6 and transfection

To evaluate the role of Gas6 in the inhibitory effect of adiponectin on calcification, we knocked down Gas6 using siRNA. Two kinds of siRNA were designed to target human Gas6 and nonspecific control siRNA was synthesized using standard templates (6). siRNA (100 nM) was transfected using transfection reagent (Upstate, Charlottesville, VA) when HASMC had reached 80–90% confluence and then was transfected every 2 d with TNFα and adiponectin up to 6 d. The efficiency of Gas6 siRNA was confirmed with immunoblotting (6).

RNA extraction and Northern blot analysis

Total RNA was extracted from HASMC using an RNeasy minikit (QIAGEN, Courtaboeuf, France). For Northern blot analysis, harvested RNA (5 μg) was fractionated on 1.4% formaldehyde-agarose gel and transferred to a nylon filter. The filter was hybridized at 68 C for 2 h with ^{32}P-labeled Gas6 cDNA (6) and an 18S probe in QuickHyb solution (Stratagene, La Jolla, CA) and autoradiographed.

Immunoblotting

The effect of TNFα and adiponectin on the expression of Gas6, phospho-Akt, and Akt was examined, as described previously (24). Analysis of AMPK activation was performed using an antibody specific for the phosphorylated Thr172 of AMPK (Cell Signaling Technology Inc., Beverly, MA).

Statistical analysis

All results are presented as mean ± SE. Statistical comparisons were made by ANOVA, followed by Bonferroni test. A value of $P < 0.05$ was considered statistically significant.

Results

Adiponectin and TNFα regulate Pi-induced calcification in HASMC

To investigate the effect of adiponectin and TNFα on Pi-induced calcification, HASMC were incubated with adiponectin and TNFα in the presence of 2.6 mM Pi. On d 6, Ca deposition was suppressed by adiponectin in a concentration-dependent manner (40 ± 2% of control at 300 ng/ml, Fig. 1A), whereas TNFα significantly augmented Ca deposition (182 ± 13% of control at 50 ng/ml; Fig. 1B). Furthermore, adiponectin clearly inhibited Ca deposition stimulated by TNFα in a concentration-dependent manner (Fig. 1C). This was also found by von Kossa's staining (Fig. 1D). These results suggest that adiponectin has an inhibitory effect on both Pi-induced and TNFα-stimulated calcification in HASMC.

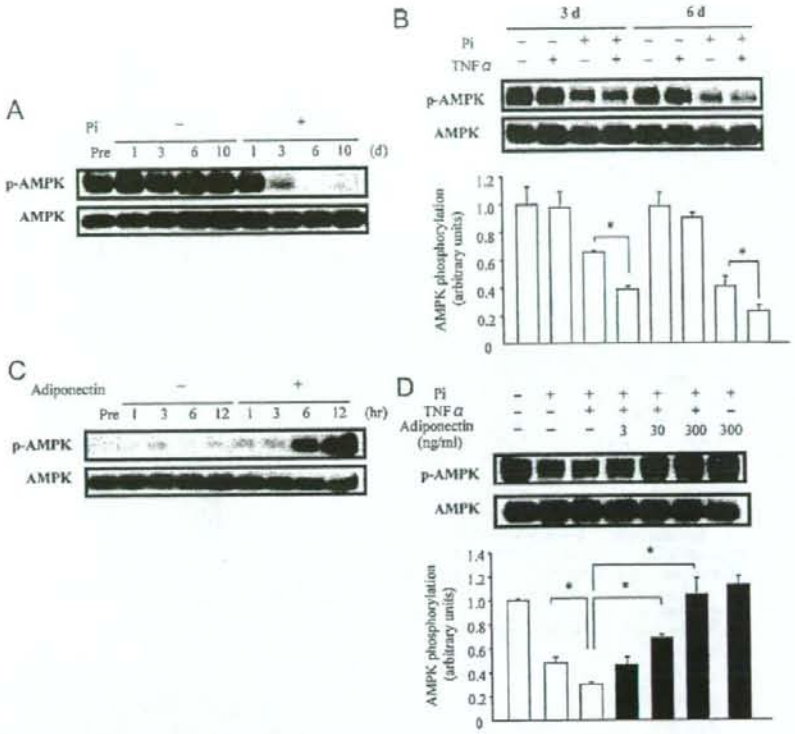

FIG. 4. Effect of adiponectin and TNFα on AMPK activity during Pi-induced calcification. HASMC were cultured in the absence or presence of Pi (2.6 mM) for up to 10 d. After the indicated incubation period, cell lysates were harvested and immunoblotted with antibodies to phospho-AMPK (p-AMPK) and AMPK. A, The untreated condition is the serum-supplemented status without Pi. B, Immunoblotting analysis showing the effect of TNFα (20 ng/ml) on p-AMPK and AMPK expression in the absence or presence of serum containing Pi (2.6 mM). C, Serum-starved HASMC were incubated with or without adiponectin (300 ng/ml) for 12 h. HASMC were cultured with the indicated concentrations of adiponectin and TNFα (20 ng/ml). D, On d 6, cell lysates were harvested and immunoblotted with antibodies to p-AMPK and AMPK. All values are presented as mean ± SE (n = 3). *, $P < 0.05$ by Bonferroni test. Each experiment was performed in triplicate for each condition.

Adiponectin antagonizes stimulatory effect of TNFα on Pi-induced apoptosis by restoration of Gas6-mediated survival pathway

Because apoptosis has been shown to be an important pathway regulating Pi-induced calcification (6, 24), we examined the effect of adiponectin and TNFα on apoptosis in HASMC. Adiponectin, at concentrations exerting inhibitory effects on calcification, significantly reduced apoptosis, as quantified by cytoplasmic histone-associated DNA fragments (Fig. 2A). On the other hand, apoptosis was enhanced by TNFα in the presence of Pi (Fig. 2B). As shown in Ca deposition, adiponectin antagonized the stimulatory effect of TNFα on apoptosis. This inhibition was also observed by TUNEL assay (Fig. 2, C and D).

We previously demonstrated that Pi-induced apoptosis was mediated by down-regulation of the Gas6-mediated survival pathway (6, 24). Therefore, we examined the effects of adiponectin and TNFα on this pathway. Both Gas6 mRNA and protein expression were down-regulated by TNFα in the presence of Pi, whereas adiponectin clearly restored their expression (Fig. 3, A and B). Next, because the Gas6-mediated survival pathway is Akt-dependent, the effect of adiponectin and TNFα on Akt phosphorylation was examined. As shown in the Gas6 expression, the similar effect of adiponectin and TNFα was observed in Akt phosphorylation that is high at basal level in the untreated condition containing serum (Fig. 3A). We confirmed that total Akt was not changed by adiponectin and TNFα treatment (Fig. 3A). On the other hand, adiponectin and TNFα did not affect Gas6 expression and Akt phosphorylation in the condition without Pi treatment (data not shown).

Furthermore, to evaluate the role of Gas6 in the inhibitory effect of adiponectin on calcification, we examined whether the knockdown of Gas6 abrogated the effects of adiponectin using siRNA. On d 6, transfection of Gas6 siRNA markedly decreased its expression (data not shown), as reported previously (6). The inhibitory effect of adiponectin on Pi- and TNFα-induced calcification was reversed by Gas6 siRNA, supporting the critical role of Gas6 in the effect of adiponectin on calcification (Fig. 3C).

AMPK plays a critical role in VSMC calcification and is regulated by adiponectin and TNFα

It has been reported that AMPK is a central signaling molecule in adiponectin's action (19, 20). We investigated whether AMPK is involved in the effect of adiponectin on Pi-induced calcification. First, we examined the activity of AMPK during calcification. Immunoblot analysis showed that phosphorylated AMPK was markedly down-regulated in the presence of Pi for 10 d, whereas the expression of total AMPK was not changed (Fig. 4A). TNFα further inhibited its phosphorylation in the presence of Pi, without changing total AMPK (Fig. 4B). In the case of adiponectin, AMPK phosphorylation was remarkably stimulated in a time-dependent manner (Fig. 4C). As shown in Fig. 4D, adiponectin further restored AMPK phos-

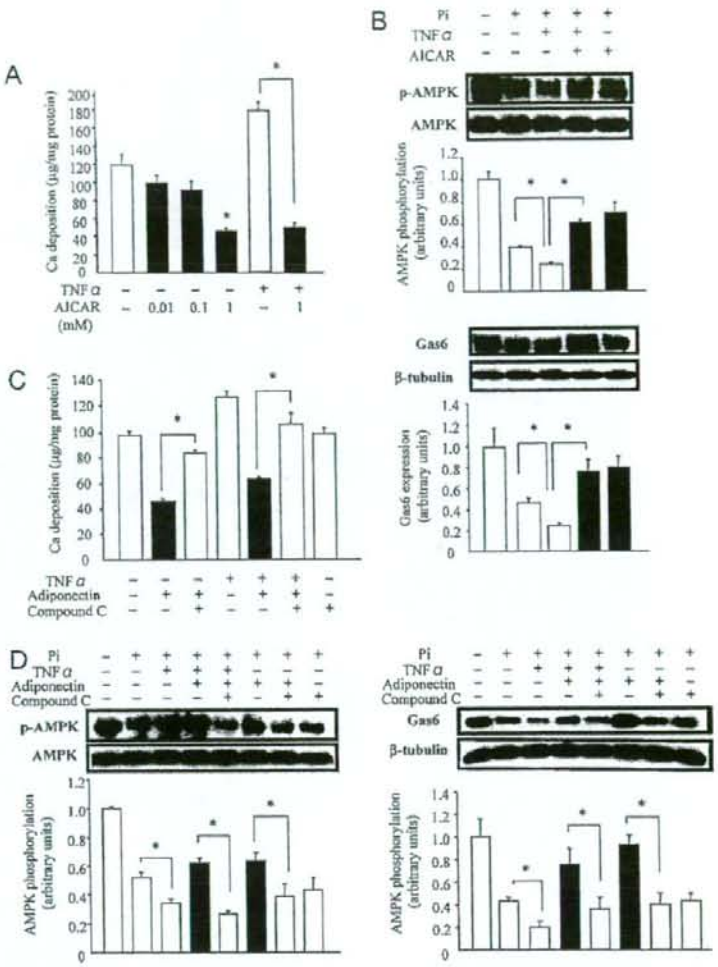

FIG. 5. AMPK plays an important role in Pi-induced calcification. HASMC were treated with or without AICAR (1 mM), a pharmacological activator of AMPK and TNFα (20 ng/ml) in calcification medium for 6 d. A and B, Ca deposition (n = 6) (A) was measured, and immunoblotting with antibodies to p-AMPK, AMPK, Gas6, and β-tubulin (B) was performed (n = 3). HASMC were cultured with or without compound C (1 μM), a chemical inhibitor of AMPK, adiponectin (300 ng/ml), and TNFα (20 ng/ml) in calcification medium for 6 d. C and D, Ca deposition (C) was evaluated (n = 6), and immunoblotting with antibodies to p-AMPK, AMPK, Gas6, and β-tubulin (D) was performed (n = 3). All values are presented as mean ± SE. *, $P < 0.05$ by Bonferroni test. Each experiment was performed in triplicate for each condition.

phorylation that was inhibited by Pi and TNFα in a calcification-promoting condition.

To clarify the causal relationship between AMPK and calcification, we tried to activate AMPK by treatment with 5-aminoimidazole-4-carboxamide ribonucleoside (AICAR) (25). In HASMC, AICAR significantly inhibited Ca deposition in a concentration-dependent manner (Fig. 5A). In addition, TNFα-stimulated Ca deposition was also blunted by AICAR. Interestingly, AICAR restored Gas6 expression down-regulated by Pi and TNFα (Fig. 5B). Next, to investigate whether the effect of adiponectin is dependent on AMPK, we tried to block AMPK using compound C, a chemical inhibitor of AMPK. As shown in Fig. 5C, compound C clearly abrogated the inhibitory effect of adiponectin both on Pi- and TNFα-induced calcification. The increase in Gas6 expression as well as AMPK phosphorylation by adiponectin was also abolished by compound C (Fig. 5D). These results suggest that AMPK regulates Gas6 expression, followed by regulation of Ca deposition in HASMC.

Transcription activity of Gas6 is regulated by adiponectin and TNFα via AMPK

To investigate whether Gas6 expression is transcriptionally regulated by adiponectin, TNFα, and AMPK, a promoter study was undertaken. Reporter assay using the −1.9-kb Gas6-luciferase DNA construct revealed that adiponectin completely reversed the down-regulation of Gas6 transcription activity by TNFα. Furthermore, compound C abrogated the effect of adiponectin on Gas6 transcription activity, indicating that adiponectin and TNFα regulate Gas6 expression at the transcription level via AMPK activity (Fig. 6).

Discussion

The present study showed that adiponectin has a protective effect against Pi-induced calcification and, furthermore,

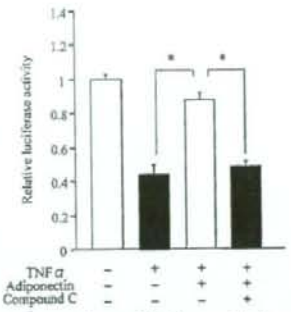

FIG. 6. Effect of adiponectin and TNFα on Gas6 promoter activity. HASMC were transfected with the Gas6 promoter-luciferase construct using lipofectamine 2000. Twenty-four hours after transfection, adiponectin (300 ng/ml), compound C (1 μM), and TNFα (20 ng/ml) were added. Cells were incubated for an additional 44 h. Luciferase activity was normalized to that of vehicle-treated cells. All values are presented as mean ± SE (n = 4). *, $P < 0.05$ by Bonferroni test. Each experiment was performed in triplicate for each condition.

has an antagonistic effect on TNFα-augmented calcification. Based on our previous finding that Pi-induced calcification is dependent on apoptotic cell death in HASMC, we examined the role of adiponectin and TNFα in Pi-induced apoptosis. As expected, we found that adiponectin had an inhibitory effect and TNFα had a stimulatory effect on Pi-induced apoptosis. This study also demonstrated the

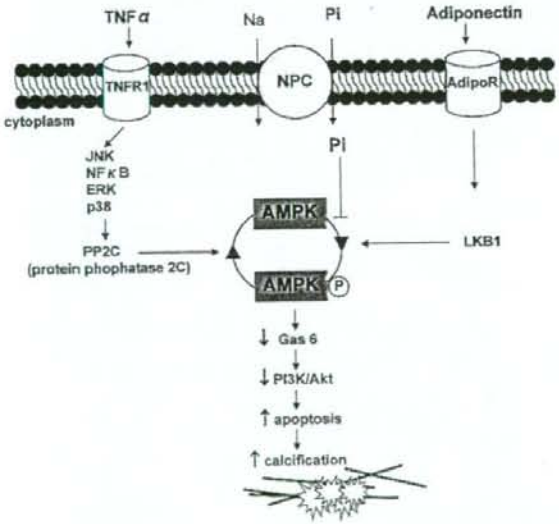

FIG. 7. Scheme of the effect of TNFα and adiponectin on Pi-induced calcification. In HASMC, exogenous Pi is internalized by sodium-dependent phosphate cotransporter (NPC, such as Pit-1) and inhibits AMPK phosphorylation, followed by down-regulation of the Gas6-mediated survival pathway. This pathway stimulates apoptosis, leading to subsequent development of calcification. TNFα directly suppresses AMPK activation by promoting PP2C activation via TNF receptor-1 (TNFR1). On the other hand, adiponectin activates LKB1-AMPK pathway via adiponectin receptors (AdipoR). AMPK activation modulated by TNFα and adiponectin contributes to the regulation of Pi-induced calcification.

regulation of Gas6 expression by TNFα and adiponectin, a suppressive effect and a promoting effect, respectively, at the transcriptional level. Akt, a critical downstream effecter of Gas6, was activated by adiponectin, whereas TNFα had an opposite action on its phosphorylation. Given that adiponectin and TNFα did not affect Gas6 expression and Akt phosphorylation in the absence of Pi (data not shown), the effects of adiponectin and TNFα on these molecules may dependent on Pi-induced responses. These results suggest that Gas6 is the target of adiponectin and TNFα in regulating Pi-induced apoptosis, accompanied by modulation of the Akt-dependent survival pathway.

As reported previously (6), Pi-induced VSMC calcification is associated with both phenotypic transition to osteoblastic cells via sodium-dependent phosphate cotransporter and apoptotic cell death. In our preliminary experiments, the expression of osteopontin, an osteoblastic marker, was not affected by TNFα and adiponectin (data not shown). Although this result suggests little influence of TNFα and adiponectin on osteoblastic differentiation of VSMC, extensive and systematic investigation including other markers of osteoblastic differentiation is needed to conclude this issue.

Multiple lines of clinical evidence show that adiponectin has protective actions on the cardiovascular system (26, 27). Circulating levels of adiponectin in humans are as high as 500–30,000 μg/ml (28). Therefore, the concentration of adiponectin (300 ng/ml) used in this study are within physiological levels. Especially, consistent with our findings, adiponectin has been implicated in apoptosis of cardiovascular cells (19, 23, 29). Adiponectin inhibits apoptosis in cardiac myocytes and fibroblasts that are exposed to hypoxia-reoxygenation stress (19). In endothelial cells, adiponectin has been reported to inhibit serum starvation-induced apoptosis (23). *In vivo* experiments have also shown that adiponectin-deficient mice develop larger myocardial infarcts due to increased myocardial cell apoptosis and TNFα expression (17). Taking these observations together with our results, the antiapoptotic actions of adiponectin contribute to the inhibition of VSMC calcification.

Most effects of adiponectin have been attributed to the activation of AMPK, which affects many aspects of cellular metabolism including glucose uptake (30, 31), glucose utilization (32), and fatty acid oxidation (33, 34). Recently, AMPK activation in VSMC has been suggested as a target to prevent or treat vascular disease (35, 36). AICAR-induced AMPK activation inhibited angiotensin II-stimulated VSMC proliferation, and administration of AICAR prevented neointimal formation in a rat balloon injury model (35). AMPK activation in VSMC elicited cell cycle arrest at the G1 phase and inhibited cell proliferation via p53 up-regulation (36). Furthermore, in the heart, the inhibitory effects of adiponectin on ischemic injury-induced apoptosis have been shown to be dependent on AMPK activation (19). The results of *in vitro* studies also revealed that AMPK signaling is essential for the antiapoptotic activities of adiponectin on endothelial cells (23). These observations are consistent with the finding of the present study that AMPK activated by adiponectin stimulated Gas6 expression to restore the survival pathway, leading to the suppression of calcification.

In the present study, we further demonstrated that adiponectin significantly augmented the transcriptional activity of Gas6